Bond between glass fibre reinforced polymer bars and high - strength concrete

Najia Saleh[a] *, Ashraf Ashour[b] and Therese Sheehan[b]
[a] Civil Engineering Department, University of Omar Al-Mukhtar, Al Baida, Libya
[b] School of Engineering, University of Bradford, Bradford, BD7 1DP, UK
E-mails: obeidinajia@hotmail.com,
a.f.ashour@bradford.ac.uk,T.sheehan@bradford.ac.uk

ABSTRACT

In this study, bond properties of glass fibre reinforced polymer (GFRP) bars embedded in high-strength concrete (HSC) were experimentally investigated using a pull-out test. The experimental program consisted of testing 84 pull-out specimens prepared according to ACI 440.3R-12 standard. The testing of the specimens was carried out considering bar diameter (9.5, 12.7 and 15.9 mm), embedment length (2.5, 5, 7.5 and 10 times bar diameter) and surface configuration (helical wrapping with slight sand coating (HW-SC) and sand coating (SC)) as the main parameters. Twelve pull-out specimens reinforced with 16 mm steel bar were also tested for comparison purposes.

Most of the specimens failed by a pull-out mode. Visual inspection of the tested specimens reinforced with GFRP (HW-SC) bars showed that the pull-out failure was due to the damage of outer bar surface, whilst the detachment of the sand coating was responsible for the bond failure of GFRP (SC) reinforced specimens. The bond stress – slip behaviour of GFRP (HW-SC) bars is different from that of GFRP (SC) bars and it was also found that GFRP (SC) bars gave a better bond performance than GFRP (HW-SC) bars. It was observed that the reduction rate of bond strength of both GFRP types with increasing the bar diameter and the embedment length was reduced in the case of high-strength concrete. Bond strength predictions obtained from ACI-440.1R, CSA-S806, CSA-S6 and

JSCE design codes were compared with the experimental results. Overall, all design guidelines were conservative in predicting bond strength of both GFRP bars in HSC and ACI predictions were closer to the tested results than other codes.

Keywords: GFRP bar; high-strength concrete; pull-out; bond behaviour and design code

1 Introduction

The use of fibre reinforced polymer (FRP) re-bars as an alternative to steel reinforcement has rapidly increased because of their excellent corrosion resistance, high tensile strength to weight ratio, good non-magnetisation properties, good fatigue properties and ease of handling. However, FRP reinforced concrete members behave differently to those reinforced with steel bars due to non- ductility of FRP bars, lower modulus of elasticity and bond strength which influence the performance of FRP reinforced concrete members. The mechanism of bond stress transfer between FRP bars and concrete is a fundamental requirement to guarantee their successful application in concrete members. In addition, the use of high-strength concretes has been recently increased owing to their higher compressive and tensile strengths, better durability and higher stiffness than normal-strength concretes. Many studies have been conducted to investigate the bond behaviour of GFRP bars in normal-strength concrete (NSC) using a pull-out test [1-10]. However, very limited research studies are available in the literature regarding the bond behaviour of GFRP bars embedded in high- strength concrete using a pull-out method [5, 10-15]. Baena et al. [5] tested pull-out specimens reinforced with GFRP bars having various surface treatments (sand coating, helical wrapping with a slight sand coating and grooves) and concrete compressive strengths (30 and 50 MPa). They confirmed that different bond mechanisms were observed for different surface configurations. Moreover, the effect of surface treatment on bond strength was less significant for concretes with low compressive strengths, but it was important for concretes with high-compressive strengths [5]. The influence of two types of GFRP bar (sand coating and helical wrapping with a slight sand coating) on the bond performance was also investigated by Davalos et al. [11] considering concrete compressive strength in the range of 57 to 63 MPa. They found that sand coated GFRP bars had better bond strength than helically wrapped GFRP bars. On the contrary, the results obtained by Lee et al. [12] indicated that the bond strength for the helically wrapped with slightly sand coated GFRP bars was higher than that for the sand coated GFRP bars for concrete compressive strengths (25, 40 and 70 MPa). Hossain et al. [13] tested the bond behaviour of sand-coated GFRP bars in HSC (74 MPa) with taking into account two the effect of two parameters: bar diameter (15.9 and 19.1 mm) and embedment length (3, 5, 7, 10 times bar diameter). Their findings showed that the reduction in bond strength with increasing bar diameter was clear for each embedment length. It was also observed that the decrease rate in bond strength reduced, as the embedment length increased. Furthermore, the experimental investigation performed by Tekle et al. [14] indicated that the increase of the embedment length of sand-coated GFRP bars embedded in HSC (42 MPa) resulted in reducing in the bond strength. Lee et al. [15] investigated the effect of bar diameter (19 and 25 mm) on the bond behaviour of two types of GFRP bars (sand-coated and spiral-wrapped) in high -strength concrete (40 and 60 MPa). It was found that a reduction rate in bond strength for both GFRP types was lower with increasing the bar size. Lee et al. [10] studied the influence of concrete strength on the bond failure mode of helically wrapped and sand coated GFRP bars. They found that bond failure occurred at the interface between concrete and outer bar surface for normal strength concrete, while it occurred at the interface between outer bar surface and bar core in the case of high-strength concrete. They also found that bond strength increased with increasing the concrete strength (from 25.6 to 92.4 MPa) and this improvement in bond strength was greater in steel bars than in GFRP bars. As a result, the investigation of bond properties of GFRP bars in HSC with considering the effect of bar diameter, embedment length and bar surface has not been adequately covered in the literature. Therefore, further research needs to be conducted.

According to the previous experimental investigations [1, 2, 4, 5, 16-20], it was found that bond strength of GFRP bars in conventional concrete depends on several parameters, such as bar diameter, embedment length, compressive concrete strength, surface configuration, bar type, concrete cover, bar position and transverse reinforcement. Table 1 summarizes the parameters that influence the bond strength considered in the design guidelines (ACI 440.1R [21], CSA-S806 [22], CSA-S6 [23] and JSCE [24]). The key factors, namely concrete strength, bar diameter, concrete cover and bar position, are considered in all of these codes. Embedment length is only taken into account by ACI-440.1R-15. The bar surface is one of the main factors which affects bond strength, however, Canadian codes only considered this influence by suggesting the bar surface factor in their equations. Although each FRP type has different bond characteristics, all codes neglected the effect of fibre type on bond strength, except the Canadian codes. Furthermore, confinement provided by transverse reinforcement (stirrups) along the* developed and spliced reinforcing bars, that contributes in increasing bond strength, is considered by Japanese and Canadian (CSA-S6) codes, and it is ignored in other codes. The performance of code equations in predicting the bond strength of GFRP (HW-SC) and GFRP (SC) re-bars embedded in high - strength concrete needs to be investigated.

In this paper, the results of 84 pull-out tests performed according to ACI 440.3R-12 [25] are presented with the aim of better understanding the bond properties of two common

GFRP bar types (helical wrapping with a slight sand coating and sand coating) in high – strength concrete. The bond behaviour is analysed considering the effect of the following parameters (embedment length, bar diameter and surface configuration) on bond strength. The code predictions are compared with the test results for validating their applicability in the case of high – strength concrete.

Table 1 - Main factors considered in determining bond strength by design codes

Model	Bar diameter	Concrete strength	Concrete cover	Bar surface	Bar location	Bonded length	Transverse reinforcement	Fibre type
JSCE 1997	✓	✓	✓	x	✓	x	✓	x
CSA-S806-12	✓	✓	✓	✓	✓	x	x	✓
CSA-S6-14	✓	✓	✓	✓	✓	x	✓	✓
ACI 440.1R-15	✓	✓	✓	x	✓	✓	x	x

2 Experimental investigation

2.1 Materials

Pull-out cubes were constructed using ready – mixed concrete with a maximum coarse aggregate size of 10 mm. Cylinder specimens (150 x 300 mm) and cube specimens (100 x 100 x 100 mm) were cast and cured under the same conditions as pull-out cubes. The cylinders and cubes were tested immediately after testing the pull-out specimens to provide the splitting tensile strength and the cube compressive strength of concrete. GFRP (HW-SC), GFRP (SC) and steel bars were used in this study. Helically wrapped with slightly sand coated GFRP and sand coated GFRP bars shown in Figure 1 were made of continuous longitudinal fibres impregnated in vinylester resin: the minimum content of continuous ECR-glass fibres was 75% (per weight) and the maximum content of vinylester resin was 25%, and the content of continuous E-glass fibres 80% (per unit weight) and vinylester resin 20%, respectively. The tensile strength and elastic modulus of GFRP and steel bars were determined according to specifications ASTM

D7205/D7205M [26] and ASTM A706/A706M [27], respectively. The outer diameters were measured according to ACI 440.3R-12 [25]. The geometrical and mechanical properties of GFRP and steel bars are summarized in Table 2, and the mechanical properties of vinylester resin are shown in Table 3.

Table 2. Geometrical and mechanical properties of GFRP and steel bars

Bar type	GFRP (HW-SC)			GFRP (SC)			Steel
Bar size	3#	4#	5#	3#	4#	5#	5#
Nominal diameter (mm)	9.5	12.7	15.9	9.5	12.7	15.9	16
Measured diameter (mm)	10.76	13.44	16.76	10.4	13.33	16.74	-
Tensile strength (MPa)	827 (940.2)	758 (797)	724 (867.9)	1227.3 (1224.6)	1375 (1175.4)	1373.7 (1210.3)	672 (666)
Ultimate strain (%)	1.79	1.64	1.57	2.4	2.7	2.7	-
Elastic of modulus (GPa)	46 (51.7)	46 (49.7)	46 (46.9)	50 (50.98)	51 (51.57)	51 (52.15)	200 (199)
Yielding strength (MPa)	-	-	-	-	-	-	582 (569)

The values between brackets measured in the laboratory are the average of three samples, whereas other values are provided by the manufacturer.

Table 3. Mechanical properties of vinylester resin

Bar type	Flexural Strength (MPa)	Flexural Modulus (MPa)	Tensile Strength (MPa)	Tensile Elongation (%)	Tensile Modulus (MPa)
GFRP (HW-SC)	144	3500	84	4.2	3400
GFRP (SC)	156	3172	90	4.2	3586

(a) Helically wrapped with sand coated surface (type A)

(b) Sand coated surface (type B)

Figure 1. Surface configurations of GFRP re-bars

2.2 Test specimens

Seventy-two GFRP and twelve steel reinforced cubes were tested. The parameters investigated were bar diameter (9.5, 12.7 and 15.9 mm for GFRP and 16 mm for steel) and embedment length (2.5, 5, 7.5 and 10 times bar diameter). The geometrical details of the pull-out cubes are given in Figure 2. The un-bonded length was covered by a PVC tube to prevent contact between the bar and the concrete. The concrete mix (C1) was used to cast cubes reinforced with GFRP (type A) and steel reinforced concrete cubes having embedment lengths $2.5d_b$ and $5d_b$. Specimens reinforced with GFRP (type B) and those reinforced with steel bars having embedment lengths $7.5d_b$ and $10d_b$ were cast using the second batch (C2). Before casting, the inner sides of the moulds were covered by a thin film of oil to allow demoulding of the specimens. The concrete was placed in three layers and each layer was vibrated using a poker vibrator. After casting, all specimens were covered with a polythene sheet to prevent evaporation of water from the unhardened concrete until demoulding. After one week, the specimens were demoulded, marked, covered with a polythene sheet and stored in a temperature-controlled laboratory until testing.

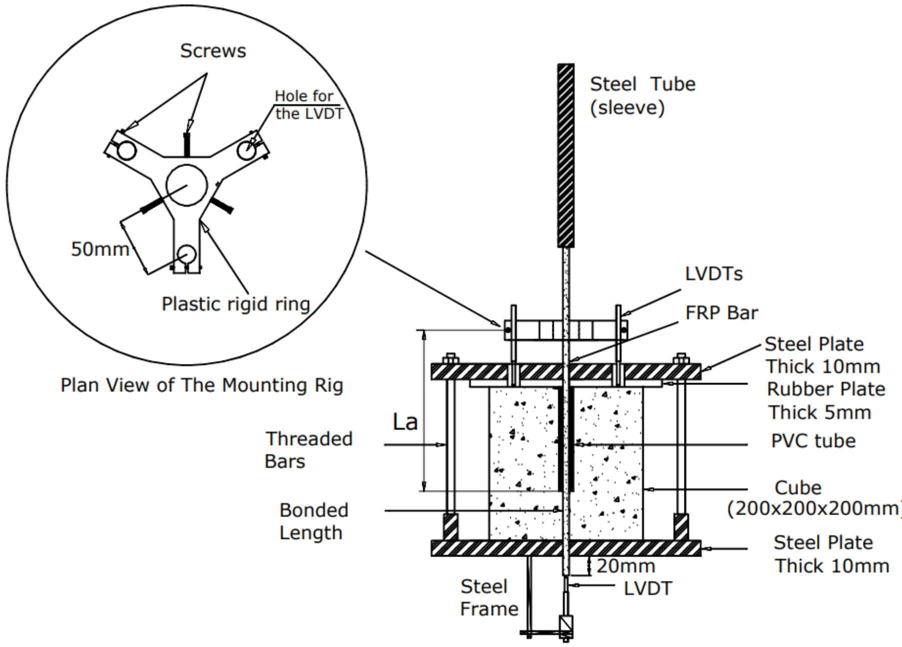

Figure 2. Pull-out test arrangement

2.3 Experimental set-up

The pull-out test set-up is shown in Figure 3. The specimen was placed in a specially made steel frame that was positioned in the testing machine. Three linear variable displacement transducers (LVDTs) were connected to the bar by a plastic rigid rig and touched the top surface of the specimen to measure the loaded end slip. Only one LVDT was attached to a small steel frame which was fixed to the below surface of the concrete cube to measure the free end slip. Small irregularities at the top surface of the cube might result in accidental bending of the bar during loading or movements caused by local crushing. Therefore, a 5-mm-thick rubber plate was introduced to secure the contact between the top surface of the concrete block and the steel bearing plate. The tensile load was applied directly to the bar using a testing machine of 500 kN capacity. The loading rate was changed for each 15 mm of head movement of the machine to be 0.02, 0.05 and 0.1 mm/sec, respectively. The reason for increasing the loading rate was to accelerate the test after the occurrence of pull-out failure. The displacement-control mode was selected to record the post-peak curve. Applied load and LVDT readings were automatically recorded using the data logging system.

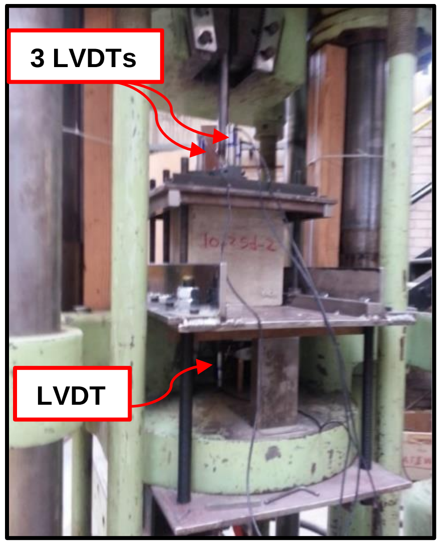

Figure 3. Pull-out test set-up

3 Test results and discussion

Three identical specimens for each configuration were tested. The bond stress - slip relationships were developed and plotted using measured data. The bond stress is defined by equation 1.

$$\tau = \frac{F}{\pi \mathrm{d_b} \mathrm{l_e}} \tag{1}$$

where τ is the bond stress (N/mm^2); F is the applied tensile load (N); $\mathrm{d_b}$ is the bar diameter (mm) and $\mathrm{l_e}$ is the embedment length (mm). As the three LVDTs readings at the loaded end of the bar covered both the loaded end slip and the elastic elongation of the bar above the embedment length (L_a) (see Figure 2), therefore, the loaded end slip (s_{le}) is calculated by subtracting the LVDT measurement (s_{total}) from the bar extension (s_e) as illustrated in equations 2 and 3:

$$s_{le} = s_{total} - s_e \quad (2)$$

$$s_e = \frac{F.L_a}{A_b.E_{frp}} \quad (3)$$

where A_b is the cross-sectional area of bar (mm^2), L_a is the length from the LVDTs support point to the top surface of the bonded bar (mm) (see Figure 2) and E_{frp} is the elastic modulus of the bar (MPa). The displacement at the unloaded end of bar was directly obtained from the slip measurement of the bottom LVDT. The maximum applied load (F_{max}), the maximum bond strength (τ_{max}) with the corresponding loaded end slip (s_{le}) and unloaded end slip (s_{ul}), failure mode, the average compressive strength of four concrete cubes (f_{cu}) and average splitting tensile strength of three concrete cylinders (f_t) are presented for specimens reinforced with type A and type B in Tables 4 and 5, respectively. The mean values of bond strength (τ_{avg}) and the corresponding loaded end and free end slips ($s_{le,m}$ and $s_{ul,m}$) (obtained as an average of the results of three identical specimens) are also reported. The cube compressive strength of concrete C1 was in the range of 97.38 to 102.36 MPa with an average of 100.17 MPa and a coefficient of variation (COV) of 2.4%. As for concrete C2, it changed from 77.47 to 83.07 MPa with an average of 79.24 MPa and a COV of 2.9%. The average splitting tensile strength of concrete C1 and C2 obtained from testing three cylinders varied from 4.13 MPa to 4.71 MPa with an average of 4.34 MPa and a COV of 7.3% and changed from 3.24 MPa to 3.67 MPa with an average of 3.46 MPa and a COV of 6.2%, respectively. A small difference was observed among the bond strengths of the three identical cubes because of the non-homogenous nature of conventional concrete. The definition of specimen notation is as follows: the first letter denotes the bar type (A for GFRP (HW-SC), B for GFRP (SC) and C for steel); the first number indicates the bar diameter; the second one denotes the embedment length and the last number refers to the specimen number.

Table 4. Experimental results of pull-out cubes reinforced with GFRP (HW-SC) bars in concrete C1

Specimen label	f_{cu} (MPa)	f_t (MPa)	F_{max} (kN)	τ_{max} (MPa)	S_{ul} (mm)	S_{le} (mm)	τ_{avg} (MPa)	$S_{ul,m}$ (mm)	$S_{le,m}$ (mm)	Failure Mode
A-9.5-2.5d-1	97.38	4.13	14.95	21.09	0.434	0.531				PO
A-9.5-2.5d-2	97.38	4.13	14.11	19.9	0.193	0.228	20.55	0.306	0.416	PO
A-9.5-2.5d-3	97.38	4.13	14.64	20.66	0.291	0.490				PO
A-9.5-5d-1	97.38	4.13	28.47	20.08	0.124	0.378				PO
A-9.5-5d-2	97.38	4.13	27.83	19.63	0.391	0.659	20.08	0.211	0.448	PO
A-9.5-5d-3	97.38	4.13	29.11	20.53	0.118	0.309				PO
A-9.5-7.5d-1	97.38	4.13	The testing machine suddenly stopped before debonding failure							
A-9.5-7.5d-2	97.38	4.13	41.98	19.73	0.104	1.127	19.76	0.106	0.898	PO
A-9.5-7.5d-3	97.38	4.13	42.1	19.79	0.108	0.67				PO
A-9.5-10d-1	97.38	4.13	55.7	19.65	0.411	1.486				PO
A-9.5-10d-2	97.38	4.13	55.3	19.49	0.659	1.477	19.27	0.621	1.620	PO
A-9.5-10d-3	97.38	4.13	53	18.68	0.793	1.897				PO
A-12.7-2.5d-1	97.72	4.19	28.26	22.3	0.407	0.436				PO
A-12.7-2.5d-2	97.72	4.19	23.01	18.16	0.75	0.80	19.79	0.486	0.547	PO
A-12.7-2.5d-3	97.72	4.19	23.95	18.90	0.301	0.405				PO
A-12.7-5d-1	97.72	4.19	41.15	16.24	6.94	7.03				PO
A-12.7-5d-2	97.72	4.19	40.61	16.02	5.99	6.151	16.13	-*	-*	PO
A-12.7-5d-3	97.72	4.19	40.86	16.13	6.387	6.446				PO
A-12.7-7.5d-1	97.72	4.19	61.60	16.20	0.506	1.338				PO
A-12.7-7.5d-2	97.72	4.19	59.04	15.53	0.736	1.139	16.71	0.679	1.215	PO
A-12.7-7.5d-3	97.72	4.19	69.90	18.39	0.797	1.169				PO
A-12.7-10d-1	97.72	4.19	77.47	15.28	0.468	1.545				PO
A-12.7-10d-2	97.72	4.19	79.94	15.77	0.744	1.798	16.05	0.728	1.612	PO
A-12.7-10d-3	97.72	4.19	86.70	17.10	0.974	1.493				PO

A-15.9-2.5d-1	101.68	4.71	42.13	21.21	0.458	0.634				PO
A-15.9-2.5d-2	101.68	4.71	38.55	19.42	0.330	0.414	19.42	0.363	0.496	PO
A-15.9-2.5d-3	101.68	4.71	35	17.62	0.302	0.440				PO
A-15.9-5d-1	101.68	4.71	70.65	17.78	0.388	1.049				PO
A-15.9-5d-2	101.68	4.71	79.04	19.90	0.826	1.111	18.70	0.60	1.097	PO
A-15.9-5d-3	101.68	4.71	73.20	18.42	0.586	1.131				PO
A-15.9-7.5d-1	102.36	4.71	97.21	16.32	0.439	1.170				PO
A-15.9-7.5d-2	102.36	4.71	98.51	16.53	0.858	1.234	16.32	0.533	1.208	PO
A-15.9-7.5d-3	102.36	4.71	96.02	16.11	0.304	1.220				PO
A-15.9-10d-1	102.36	4.71	115.5	14.55	0.410	1.561				PO
A-15.9-10d-2	102.36	4.71	116.9	14.72	0.656	1.619	14.82	0.660	1.628	PO
A-15.9-10d-3	102.36	4.71	120.7	15.20	0.915	1.706				PO
C-16-2.5d-1	97.38	4.13	76.2	37.88	0.939	1.481	38	0.766	1.444	PO
C-16-2.5d-2	97.38	4.13	76.85	38.21	0.593	1.408				PO
C-16-5d-1	101.7	4.71	120.5	29.94	-	1.924				PO
C-16-5d-2	101.7	4.71	101.4	25.20	1.534	1.804	27.56	1.534	1.864	PO
C-16-5d-3	101.7	4.71	110.8	27.55	-	1.864				PO

Note: * indicates specimens exhibited an almost yield plateau until full slip without a clear peak bond strength.

Table 5. Experimental results of pull-out cubes reinforced with GFRP (SC) bars in concrete C2

Specimen label	f_{cu} (MPa)	f_t (MPa)	F_{max} (kN)	τ_{max} (MPa)	S_{ul} (mm)	S_{le} (mm)	τ_{avg} (MPa)	$S_{ul,m}$ (mm)	$S_{le,m}$ (mm)	Failure Mode
B-9.5-2.5d-1	83.07	3.67	20.49	28.91	0.203	0.272				PO
B-9.5-2.5d-2	83.07	3.67	21.55	30.38	0.193	0.225	28.91	0.237	0.287	PO
B-9.5-2.5d-3	83.07	3.67	19.45	27.44	0.315	0.365				PO
B-9.5-5d-1	77.68	3.24	37.20	26.23	0.138	0.581				PO
B-9.5-5d-2	77.68	3.24	37.57	26.49	0.200	0.776	25.51	0.139	0.570	PO
B-9.5-5d-3	77.68	3.24	33.78	23.82	0.081	0.377				PO
B-9.5-7.5d-1	77.68	3.24	49.96	23.48	0.203	0.695	22.15	0.187	0.716	PO
B-9.5-7.5d-2	77.68	3.24	45.94	21.59	0.213	0.726				PO

B-9.5-7.5d-3	77.68	3.24	45.50	21.39	0.145	0.729				PO
B-9.5-10d-1	77.68	3.24	54	19.05	0.191	0.971				PO
B-9.5-10d-2	77.68	3.24	54.79	19.31	0.219	1.106	19.05	0.191	1.079	PO
B-9.5-10d-3	77.68	3.24	53.30	18.79	0.165	1.160				PO
B-12.7-2.5d-1	79.72	3.48	37.34	29.48	0.124	0.213				PO
B-12.7-2.5d-2	79.72	3.48	34.27	27.04	0.170	0.286	28.26	0.145	0.230	PO
B-12.7-2.5d-3	79.72	3.48	35.81	28.26	0.142	0.193				PO
B-12.7-5d-1	79.72	3.48	57.36	22.63	0.216	0.504				PO
B-12.7-5d-2	79.72	3.48	60.96	24.05	0.232	0.548	23.21	0.261	0.523	PO
B-12.7-5d-3	79.72	3.48	58.14	22.94	0.336	0.518				PO
B-12.7-7.5d-1	77.47	3.24	75.36	19.83	0.218	0.827				PO
B-12.7-7.5d-2	77.47	3.24	77.44	20.37	0.206	0.879	19.83	0.232	0.858	PO
B-12.7-7.5d-3	77.47	3.24	73.35	19.29	0.273	0.869				PO
B-12.7-10d-1	77.47	3.24	92.53	18.25	0.223	1.418				PO
B-12.7-10d-2	77.47	3.24	92.12	18.18	0.092	1.297	18.18	0.166	1.345	PO
B-12.7-10d-3	77.47	3.24	91.77	18.10	0.185	1.322				PO
B-15.9-2.5d-1	77.47	3.24	55.15	27.77	0.250	0.406				PO
B-15.9-2.5d-2	77.47	3.24	57.69	29.04	0.210	0.320	27.77	0.250	0.369	PO
B-15.9-2.5d-3	77.47	3.24	52.61	26.5	0.291	0.381				PO
B-15.9-5d-1	77.47	3.24	90.23	22.71	0.199	0.596				PO
B-15.9-5d-2	77.47	3.24	84.63	21.30	0.161	0.583	21.52	0.179	0.595	PO
B-15.9-5d-3	77.47	3.24	81.60	20.54	0.178	0.607				PO
B-15.9-7.5d-1	77.47	3.24	125.6	21.08	0.063	1.025				PO
B-15.9-7.5d-2	77.47	3.24	103.5	17.38	0.763	1.212	19.23	0.332	1.027	PO
B-15.9-7.5d-3	77.47	3.24	114.5	19.23	0.170	0.845				PO
B-15.9-10d-1	77.47	3.24	150.4	18.93	0.441	1.766				PO
B-15.9-10d-2	77.47	3.24	156.2	19.67	-	1.832	19.41	0.441	1.763	PO
B-15.9-10d-3	77.47	3.24	155.9	19.63	-	1.693				PO

C-16-7.5d-1	78.28	3.48	142	>23.54	0.281	0.646				Y
C-16-7.5d-2	78.28	3.48	142.7	>23.65	0.252	0.615	>23.1	0.199	0.587	Y
C-16-7.5d-3	78.28	3.48	134	>22.21	0.066	0.502				Y
C-16-10d-1	78.28	3.48	133.9	>16.64	0.495	0.758				Y
C-16-10d-2	78.28	3.48	131.3	>16.33	0.541	0.607	>16.60	0.446	0.740	Y
C-16-10d-3	78.28	3.48	135.4	>16.84	0.304	0.857				Y

Note: PO = Pull-out failure; SP = Splitting failure and Y = Bar yielding
(-) = Not measured (LVDT stopped)

3.1 Bond stress - slip relationship

The response of bond stress – loaded and unloaded end slips for each specimen is illustrated in Figures 4 to 6 for cubes reinforced with GFRP (type A) bars and Figures 7 to 9 for GFRP (type B) reinforced cubes. The bond stress – slip curves for cubes reinforced with steel bars are also plotted in Figure 10. The bond stress – slip relationships are presented according to bar diameter, embedment length, surface characteristics and bar type to observe the influence of these main parameters on the bond behaviour in case of high-strength concrete.

The general trend of bond stress – slip curve for GFRP (HW-SC) bars is similar to that obtained by Lee et al. [12], Baena et al. [5], Davalos et al. [11], Okelo and Yuan [2] and Vint and Sheikh [28] from testing GFRP (HW-SC) reinforced specimens. In addition, the bond stress – slip behaviour for GFRP (SC) bars is similar to that reported by Vint and Sheikh [28], Baena et al. [5], Davalos et al. [11], Hossain et al. [13], El Refai et al. [7], Lee et al. [12], Antonietta Aiello et al. [29] and Arias et al. [30] from testing GFRP (SC) reinforced specimens.

The general behaviour of the bond stress – slip relationship is described by a high initial increase in bond stress without a significant slip in both GFRP types and steel bars due to good chemical adhesion between the bar surface and the concrete. This stage describes the initial stiffness. After the chemical adhesion resistance is lost, bond stress continues to increase with increasing the applied load until the peak point, but the amount of the slip increase is small. At this stage, bearing (undulations) and friction resistances control to prevent de-bonding in GFRP (HW-SC) reinforced specimens. However, friction resistance only dominates in specimens reinforced with GFRP (SC) bars and the mechanical interlock only controls to resist the pull-out force in steel reinforced specimens. In the descending stage (after bond failure), the bond stress reduces with increasing the slip in both GFRP types, but the shape of the softening curve changes with differing surface configuration. In specimens reinforced with helically wrapped and slightly sand coated GFRP bars, bond stress degraded gradually with increasing the loaded and unloaded end slips. It was noted that the reduction rate in residual bond stresses increases with decreasing bar diameter as rib spacing of smaller diameter bars is larger than that of higher diameter bars (rib spacings = 25, 23 and 20 mm with a constant rib height for bar diameters = 9.5, 12.7 and 15.9 mm, respectively), indicating that residual bond stresses depend on bar size. As for GFRP (type B) reinforced specimens, the bond stress reduced suddenly to be almost zero with a strong slip accompanied with a loud bang (relative brittle failure and significant energy release) due to detaching of the sand coated layer. No data was recorded during that short moment. Then, bond stress started to increase again up to a certain level, followed by an increase in the slip owing to the remaining frictional resistance. The residual bond stresses produced in GFRP (SC) reinforced specimens are lower than those produced in GFRP (HW-SC) reinforced specimens due to loss of frictional resistance, when the sand coating layer was entirely stripped, leading to a smooth surface. For steel reinforced cubes that failed in a pull-out mode, the post-peak bond stresses reduced gradually similar to GFRP (HW-SC) bars, however, the reduction was faster than the reduction in GFRP (HW-SC) reinforced specimens owing to lower frictional resistance. The bond stress – slip behaviour of specimens A-12.7-5d was different from other specimens reinforced with GFRP (HW-SC) bars as specimens exhibited an almost yield plateau until full slip without a clear peak bond strength, but similar to that obtained by Baena et al. [5] and Lee et al. [12] from testing GFRP (HW-SC) reinforced specimens. This might be attributed to the wedging action resulting from the crushed concrete sticking to the front of the ribs. From the bond stress – slip curves (Figures 4 to 10), Tables 4 and 5, it can be noted that the loaded end slip is higher than the unloaded end slip at the same pull-out load, indicating that the high bond stress at the loaded end reduces gradually towards the unloaded end (non-linear distribution).

The bond strength of GFRP (SC) bars is higher than that of GFRP (HW-SC) bars, but the corresponding slip for GFRP (SC) bars is smaller than that for GFRP (HW-SC) bars, indicating that bond properties of sand coated surfaces are better than those of the helically wrapped surfaces, and the amount of slip is influenced by the bar surface. The effect of surface configuration on the slip was confirmed by Lee et al. [12] and Pepe et al. [31]. In addition, it is noticed that the loaded end slip corresponding to the maximum bond stress increases with increasing embedment length for the same bar diameter in both GFRP types and this was also reported by Pepe et al. [31] and Tekle et al. [14]. Steel reinforced cubes having embedment lengths of 7.5 and 10 times the bar diameter were failed by yielding as shown in Figure 10, because the pullout force exceeded the force causing the bar fracture.

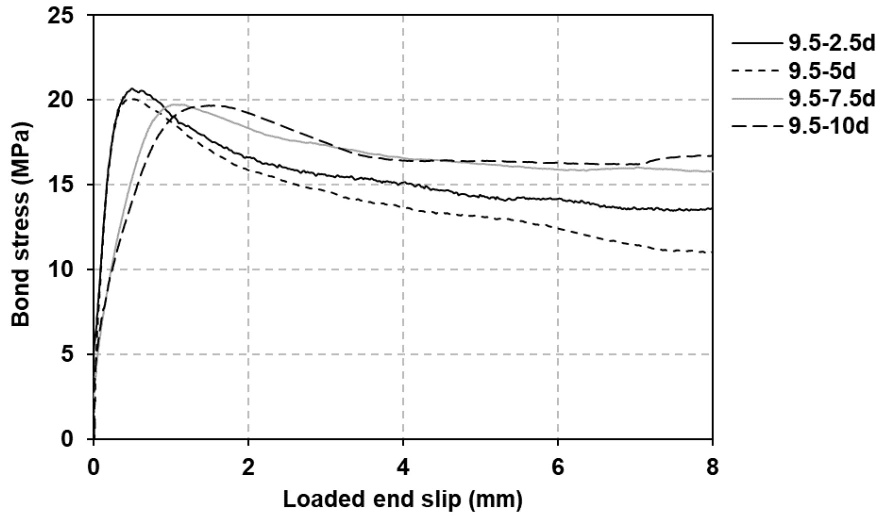

(a)

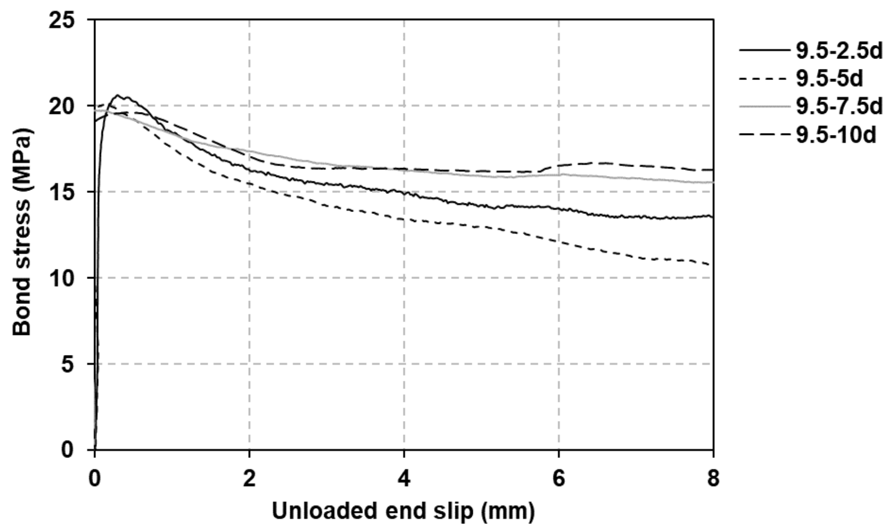

(b)

Figure 4. Bond stress - slip relationship for 9.5 mm GFRP (type A) reinforced cubes: (a) loaded and (b) unloaded end slips

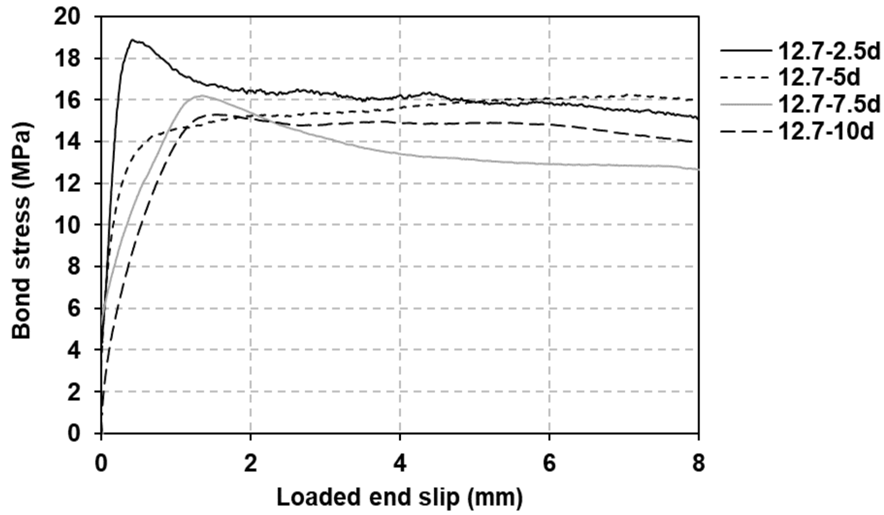

(a)

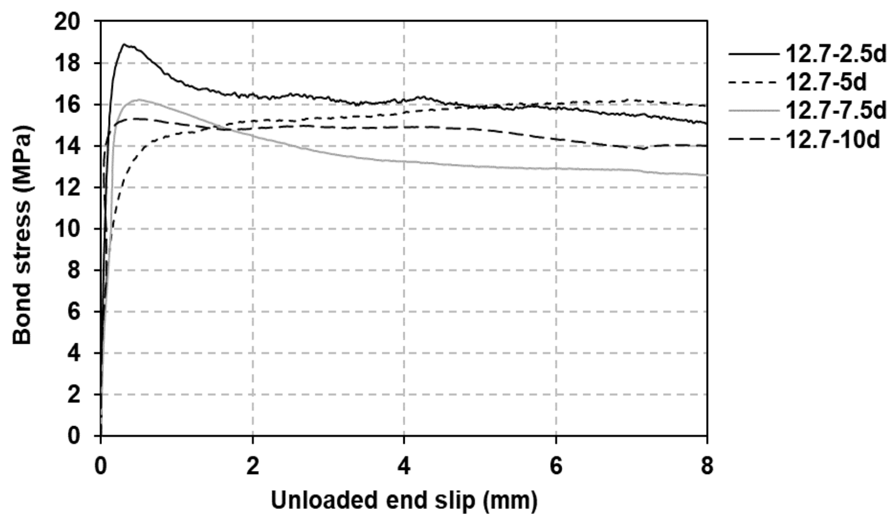

(b)

Figure 5. Bond stress - slip relationship for 12.7 mm GFRP (type A) reinforced cubes: (a) loaded and (b) unloaded end slips

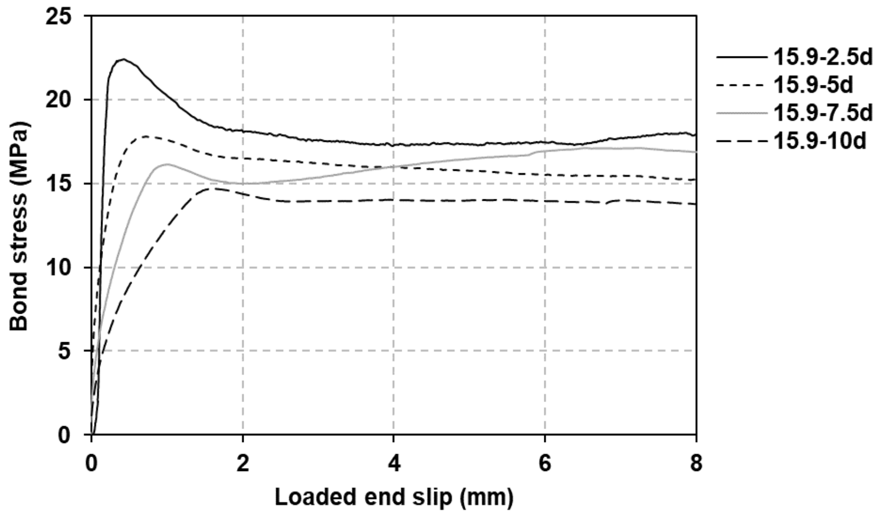

(a)

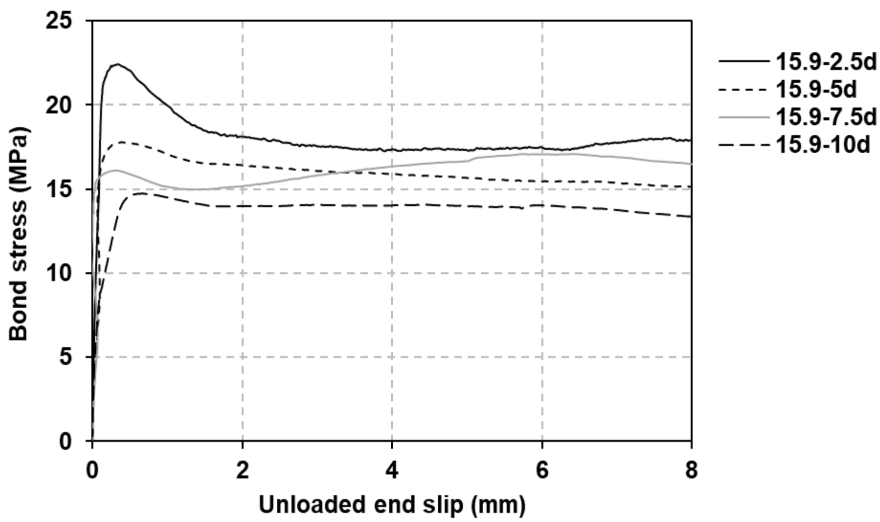

(b)

Figure 6. Bond stress - slip relationship for 15.9 mm GFRP (type A) reinforced cubes: (a) loaded and (b) unloaded end slips

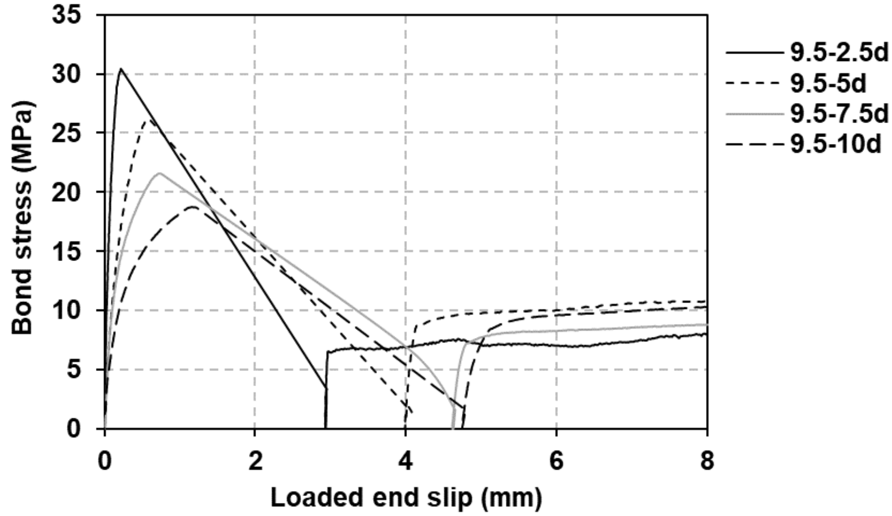

(a)

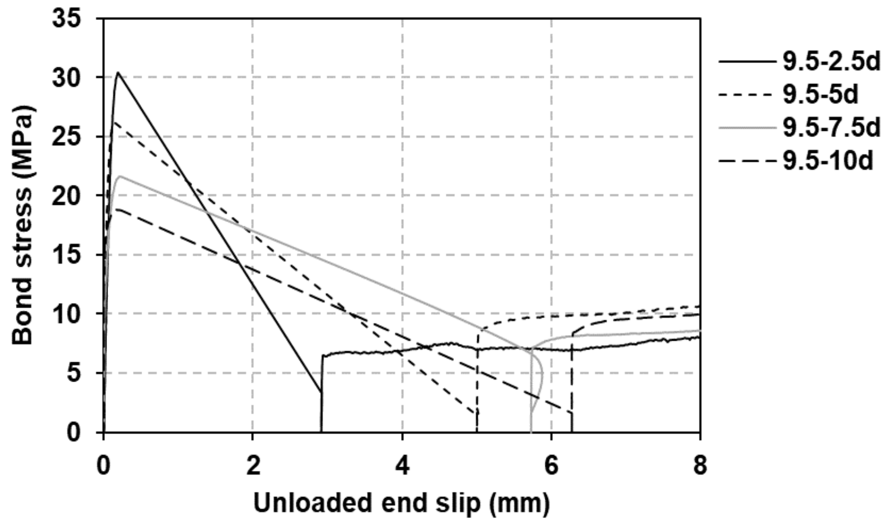

(b)

Figure 7. Bond stress - slip relationship for 9.5 mm GFRP (type B) reinforced cubes: (a) loaded and (b) unloaded end slips

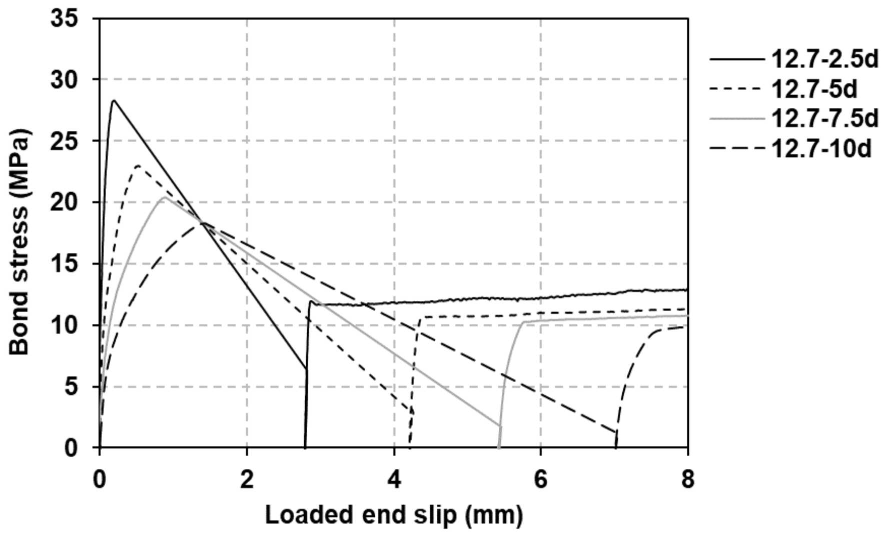

(a)

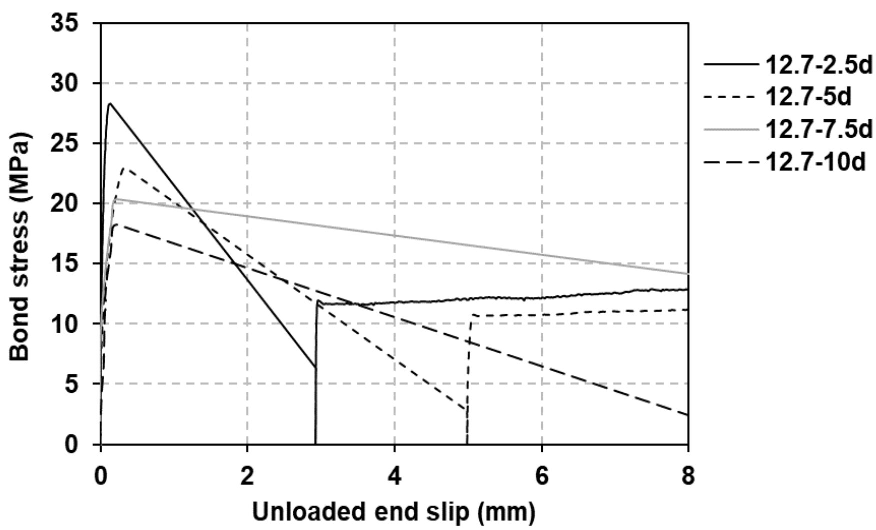

(b)

Figure 8. Bond stress - slip relationship for 12.7 mm GFRP (type B) reinforced cubes: (a) loaded and (b) unloaded end slips

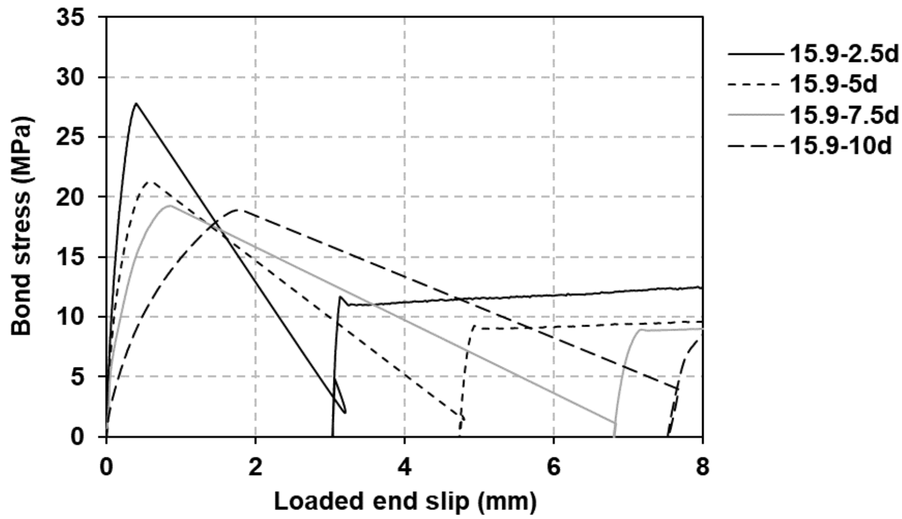

(a)

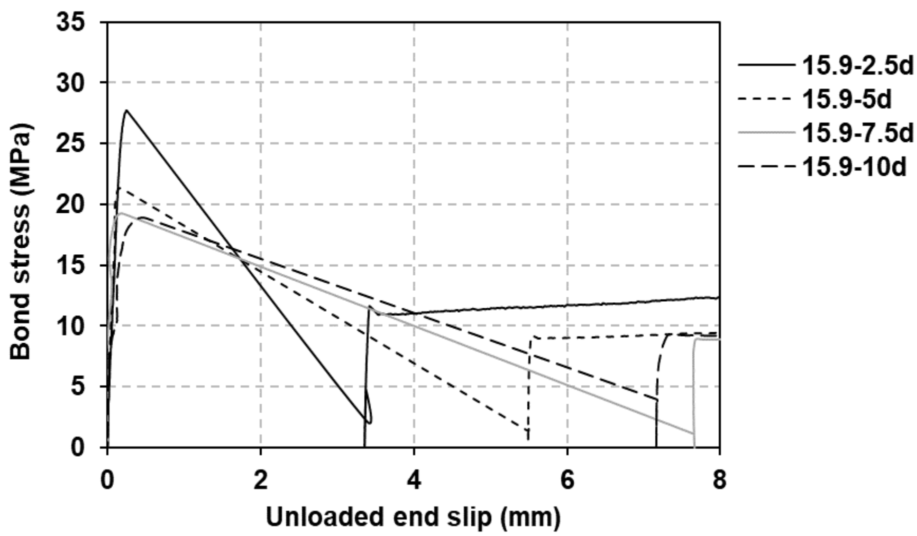

(b)

Figure 9. Bond stress - slip relationship for 15.9 mm GFRP (type B) reinforced cubes: (a) loaded and (b) unloaded end slips

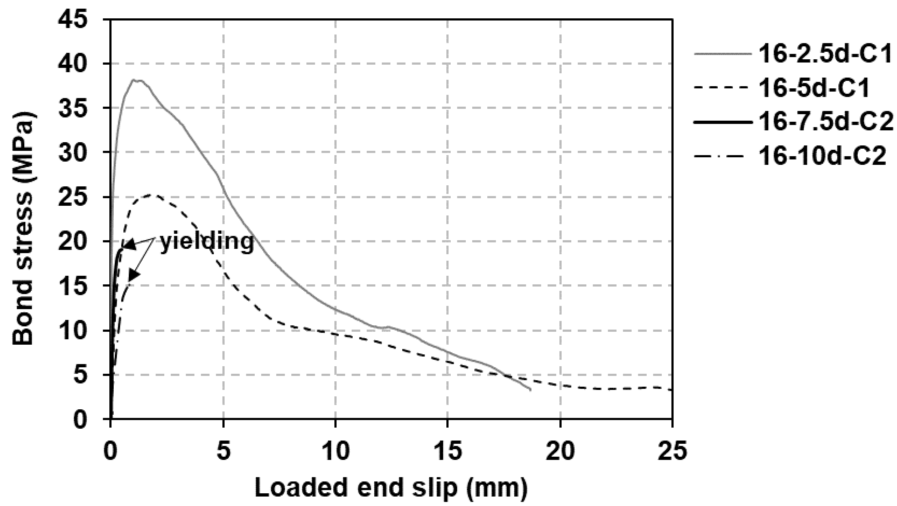

(a)

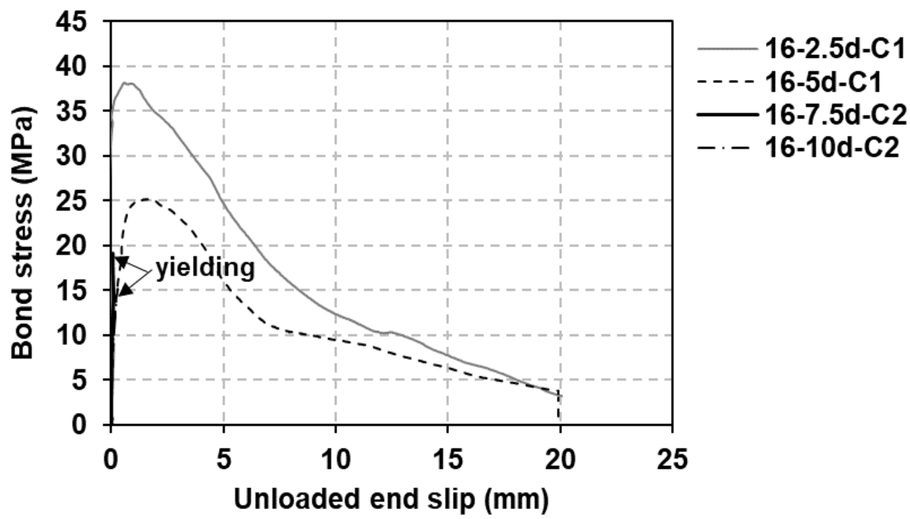

(b)

Figure 10. Bond stress - slip relationship for 16 mm steel reinforced cubes: (a) loaded and (b) unloaded end slips

3.2 Initial stiffness <u>of bond stress – slip curves</u>

Figure 11 (a and b) shows that the initial stiffness reduces with increasing the embedment length as reported by Pepe et al. [31] and Achillides and Pilakoutas [1]. This might be attributed to the non-uniform distribution of bond stresses along the bonded length. Also, it is found that the initial stiffness of steel bars is higher than that of GFRP (HW-SC) bars as shown in Figure 4.11 (a). This may be because of the differing surface properties and elastic modulus. This result was also confirmed by Baena et al. [5] from testing the pull-out cubes reinforced with different rebar types (glass FRP, carbon FRP and steel).

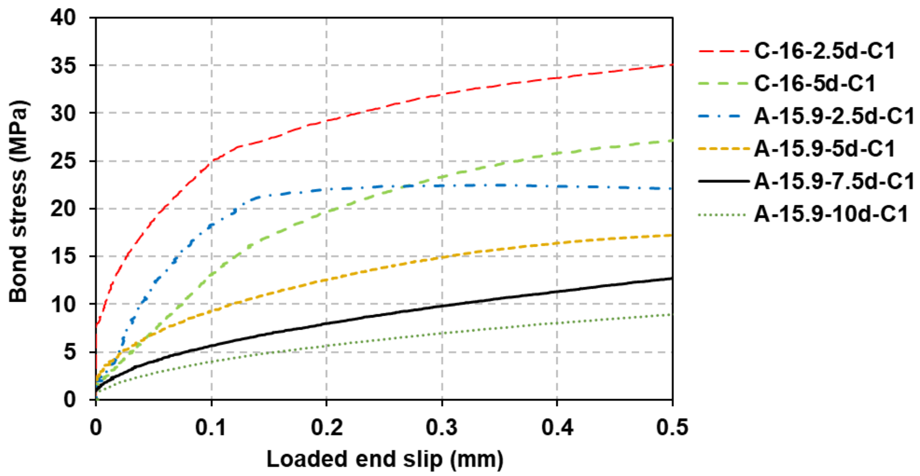

(a)

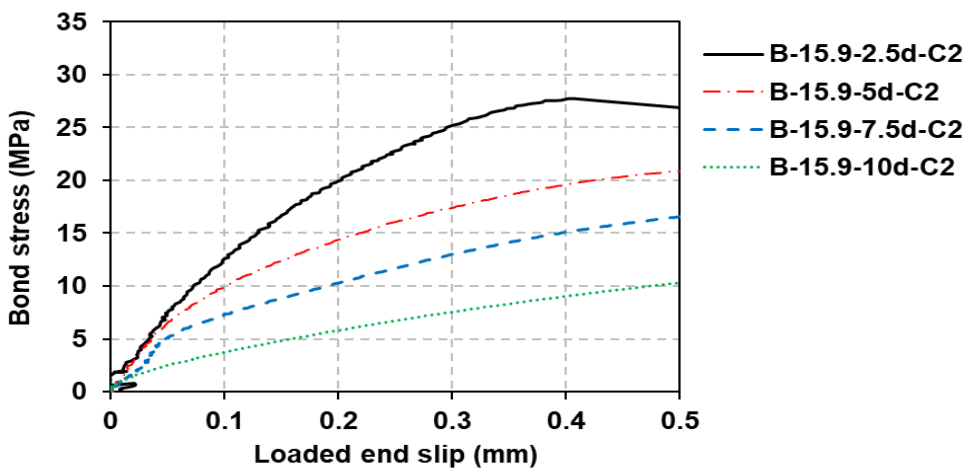

(b)

Figure 11. Influence of elastic modulus and embedment length of bar on initial stiffness

3.3 Bond failure mechanism

The failure mode observed for each pull-out test is listed in Tables 4 and 5. As anticipated, most specimens were failed by a pull-out mode as shown in Figure 12, because the cube compressive strength of concrete was designed to be higher than 80 MPa to ensure the occurrence of failure at the bar – concrete interface, rather than in the concrete. However, the specimens reinforced with steel bars, having the embedment lengths of 7.5d_b and 10d_b, failed by bar fracture before attaining the bond strength as presented in Figure 14 (b). It can be concluded that the development length required to avoid bond failure between the high-strength concrete and steel bars could be equal to or more than 7.5d_b. The specimens were split after testing to visually assess the bar and surrounding concrete conditions. As for the specimens reinforced with GFRP (HW-SC) bars, some abrasions were noted on the outer surface with stripping of sand coating as shown in Figure 13 (b). White residue was seen on the trace of the whole embedment length, which indicated crushing of the resin. As noted, the specimens with longer embedment lengths failed by damage of the fibres as illustrated in Figure 13 (a). No apparent crushing of the surrounding concrete was monitored in any of the GFRP reinforced specimens. The de-bonding failure in the sand coated GFRP reinforced specimens occurred by the entire detachment of the sand coated layer accompanied with a loud bang, when bond stress reached the peak value as demonstrated in Figure 13 (c). The concrete also remained uncrushed. This indicated that the bond strength between the outer layer and bar core was lower than that between the high-strength concrete and sand coating. Therefore, failure was controlled by the shear strength at the resin – bar core interface rather than the shear strength between the bar and concrete. This mode of failure was expected in the case of high-strength concrete. Similarity, Baena et al. [5] found that the sand coated layer was totally stripped from the GFRP-SC rebar, when the compressive strength of concrete was around 50 MPa. The specimens with a concrete strength of 30 MPa failed by a pull-out mode due to damage in the concrete surface. Concerning steel reinforced cubes failed by pull-out, Figure 14 (a) shows the remaining concrete still attached to the outer surface of steel rebar. This is an indicator that bond failure occurred by shearing off of the concrete between ribs.

Figure 12. Pull-out failure

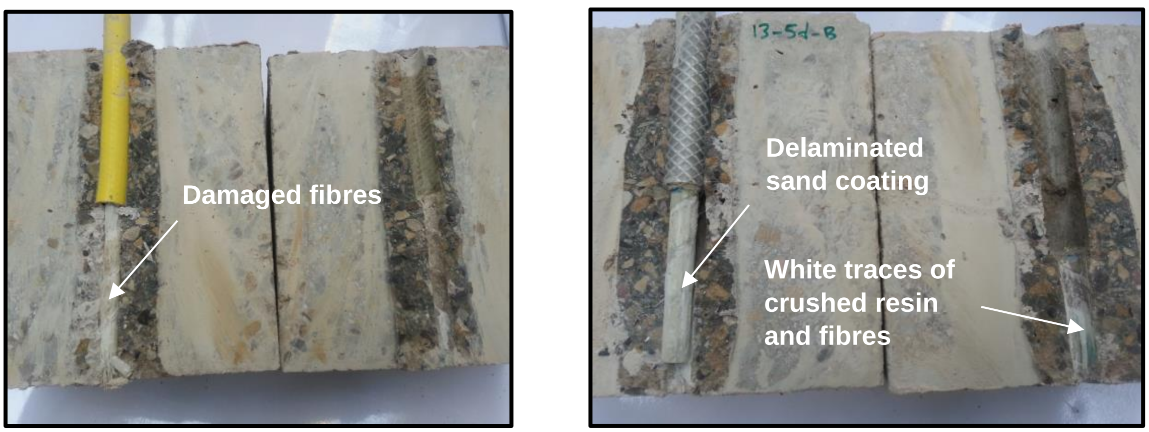

(a) Cube (A-9.5-10d) **(b) Cube (A-12.7-5d)**

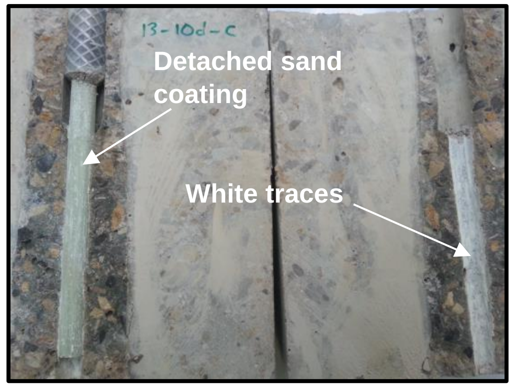

(c) Cube (B-12.7-10d)

Figure 13. Visual inspection for the specimens failed by pull-out

(a) Shear off concrete in cube (C-16-2.5d) **(b) Bar Fracture**

Figure 14. Visual inspection of specimens reinforced with steel bars

3.4 Factors influencing bond strength

3.4.1 Effect of embedment length on bond strength

Generally, the trend of the test results points out that the longer the embedment length, the smaller the value of the average bond strength, irrespective of bar diameter in both GFRP types as well as steel bars. On the other hand, as expected, the failure load increases with increasing the embedment length. The relationships between the bond strength and embedment length are shown in Figures 15 and 16 for GFRP (type A) and GFRP (type B) reinforced cubes with different bar diameters, respectively. Based on the experimental results, it can be reported that the bond strength increases with reducing the bonded length and this observation was also confirmed by some previous authors [1, 2, 7, 13, 14]. This is attributed to two main factors: 1) non-linear distribution of bond stress along the embedment length, and 2) the reduction in the bar size due to the Poisson's ratio effect, leading to reductions in the frictional and mechanical interlock resistances along the embedment length. In Figure 15, it is noted that no significant change occurred in the bond strength with the increase of embedment length for smaller bar diameters. For example, the bond strength of a 9.5 mm GFRP (HW-SC) bar having an embedment length of 10 d_b is reduced by approximately 6% compared to that having an embedment length of 2.5 d_b. However, for larger bar diameters, the reduction rates in the bond strength of 10 d_b specimens were 19% and 24% compared to 2.5d_b specimens, for 12.7 and 15.9 mm bar diameters, respectively. In Figure 16, the bond strength of 10 d_b specimens having 9.5, 12.7 and 15.9 mm diameters is decreased by almost 34%, 36% and 32% in comparison with 2.5 d_b specimens, respectively. In general, the reduction rate in bond strength of GFRP (type B) is higher than the reduction rate in bond strength of GFRP (type A). For comparison purposes, steel reinforced specimens also were tested to compare their bond strength with those reinforced with GFRP re-bars. It was found that the bond strength of GFRP (type A) bars was lower (50 to 65%) than that of steel bars, depending on embedment length. This is because of different mechanical properties and surface configurations. Regarding 7.5d_b and 10d_b steel reinforced cubes, the failure observed was a bar rupture instead of a pull-out bar. Subsequently, these specimens did not compare with counterparts reinforced with GFRP (type B) bars. It was noticed that the loaded end slip increased with increasing the embedment length for the same bar diameter in both GFRP types. The same observation was reported by Pepe et al. [31] from testing hinged beams and Tekle et al. [14] from testing pullout specimens.

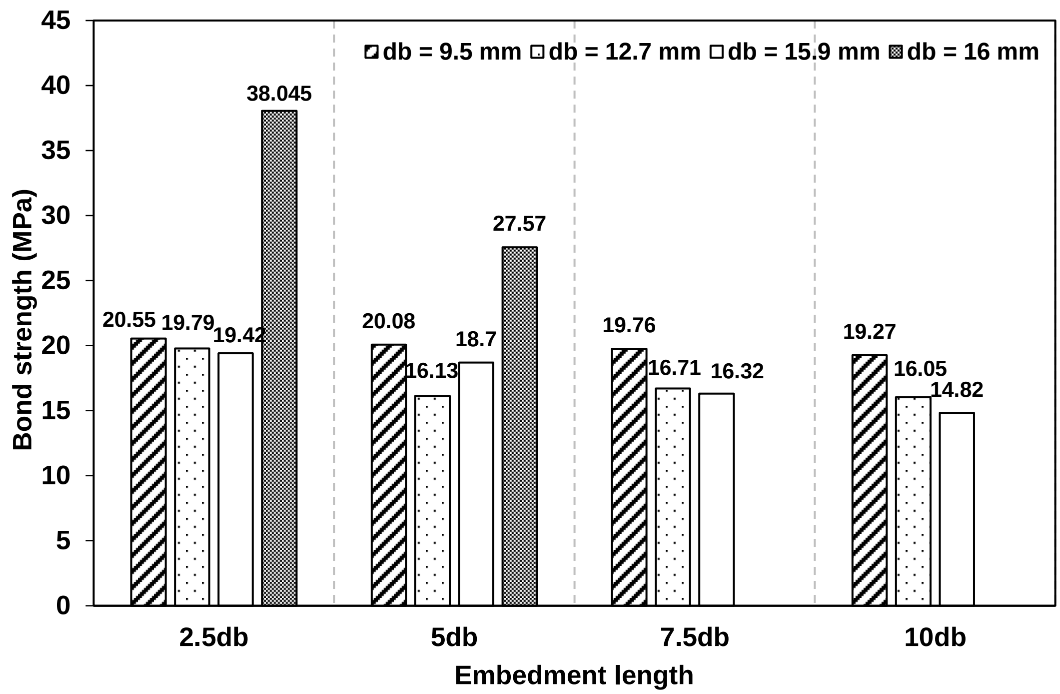

Figure 15. Effect of the embedment length and bar diameter on the average bond strength of GFRP (HW-SC) bars embedded in HSC cubes

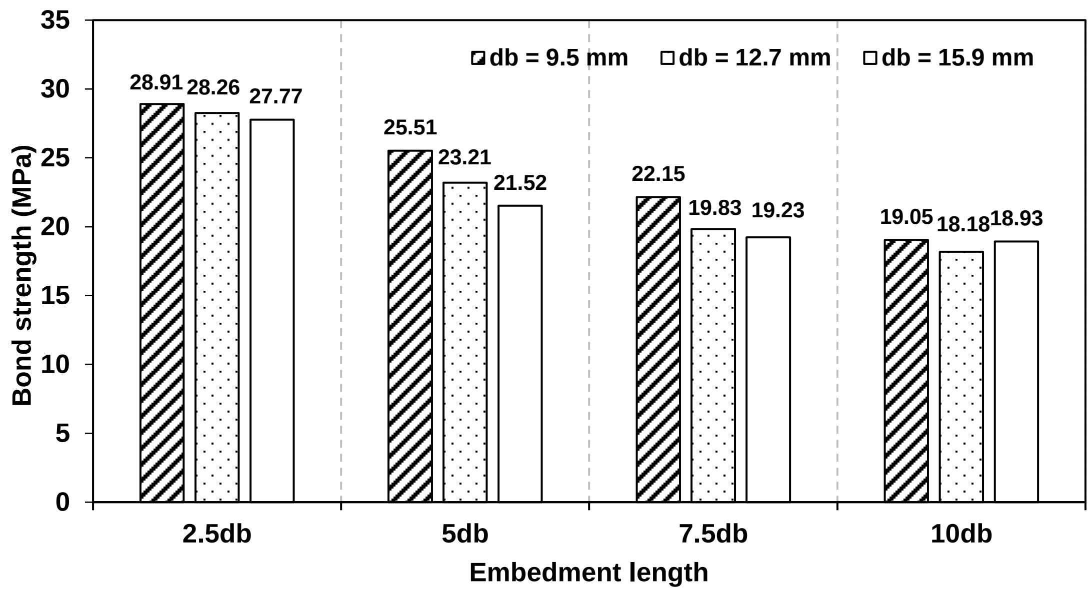

Figure 16. Effect of the embedment length and bar diameter on the average bond strength of GFRP (SC) bars embedded in HSC cubes

3.4.2 Effect of the bar diameter on bond strength

As shown in Figures 15 and 16, the average bond strength of GFRP bars reduces with increasing the bar diameter similar to steel bars. This observation is valid for all test specimens regardless of the embedment length. This trend was also reported by Nanni et al. [32], Benmokrane et al. [33], Cosenza et al. [34], Tighiouart et al. [16], Achillides [35], Achillides and Pilakoutas [1], Okelo and Yuan [2], Tepfers [36], Xue et al. [37], Baena et al. [5], Hossain et al. [13], El Refai et al. [7] and Lee et al. [15]. This is attributed to the nonlinear distribution of bond stresses along the embedment length [1, 5, 33], which is more pronounced in larger bar diameters as longer embedment lengths are required. In addition, Achillides and Pilakoutas [1] reported that the Poisson effect may have an effect on this behaviour by reducing the bar diameter subjected to the pull-out load; this reduction in bar diameter increases with the bar size. Subsequently, the frictional and mechanical interlock stresses decrease along the embedment length. Shear lag was also considered as a factor in explaining this phenomenon. The non-linear distribution of normal stresses through the cross-section of the bar increases with increasing bar diameter with normal stresses at bar surface higher than those closer to centre, violating the average bond strength [1]. From Figure 15, GFRP (type A) bars with 9.5 mm diameters showed bond strengths 5.5%, 6.9%, 17.4% and 23.1% higher than the bond strengths developed by the 15.9 mm diameters for the embedment lengths of 2.5, 5, 7.5 and 10 times the bar diameter, respectively, with an average increase of 13.2%. It can be stated that the decrease of bar diameter led to a slight increase in the bond strength for the shorter embedment lengths. These percentages were 3.7%, 19.6%, 15.4% and 16.7% more than the bond strengths developed by the 12.7 mm bar diameters for the same embedment lengths, with an average increase of 13.8%. As can be seen in Figure 16, GFRP (type B) bars with 12.7 mm bar diameters showed bond strengths that were 2.3%, 9%, 10.4% and 4.5% lower than those developed by 9.5 mm bar diameters for the embedment lengths of 2.5, 5, 7.5 and 10 times the bar diameter, respectively, with an average reduction of 6.5%. As for 15.9 mm diameters, these percentages were 4.1%, 18.5%, 15.2% and 0.6% less than those developed by 9.5 mm diameters for the same embedment lengths, with an average reduction of 9.6%. For high-strength concrete pull-out cubes, it was noticed that a reduction rate in bond strength reduced with increasing the bar diameter for all embedment lengths. A similar observation was confirmed by Lee et al. [15] and they also reported that the influence of bar diameter on bond strength was affected by concrete compressive strength.

3.4.3 Effect of bar surface treatment on bond strength

Due to the important influence of the surface properties on bond behaviour, it is worth comparing the bond performance of different surface treatments. From Figure 17, it can be seen that the bond strength of GFRP (SC) bars is higher than that of GFRP (HW-SC) bars due to their sand coated surface, which is similar to the results obtained from testing pull-out specimens for cylinder compressive strengths of concrete in the range of 57 to 63 MPa [11]. The bond strength of GFRP (SC) bars strongly depends on friction resistance provided by surface treatment, while little bearing resistance was provided by GFRP (HW-SC) bars, unlike steel bars. However, according to the findings of Baena et al. [5], the bond strength of GFRP (HW-SC) bars was higher than that of GFRP (SC) bars for a concrete strength of 53 MPa, despite the fact that the GFRP bars used were similar to the GFRP bars used in the current study. Moreover, Baena et al. [5] reported that the influence of bar surface configurations on bond strength depended on concrete strength, where the effect was less important in low - strength concrete compared to high - strength concrete. In addition, Lee et al. [12] found that bond strengths achieved by GFRP (HW-SC) re-bars were greater than those achieved by GFRP (SC) re-bars for different concrete strengths of 25, 40 and 70 MPa. As illustrated in Figure 17, the ratio of GFRP (type B) bond strength to GFRP (type A) bond strength varied from 0.99 to 1.44 with an average of 1.25, depending on bar diameter and embedment length. It was also noted that the corresponding loaded end slip in GFRP (SC) bars is smaller than that in GFRP (HW-SC) bars as shown in Tables 4 and 5. The same observation was reported by Lee et al. [12].

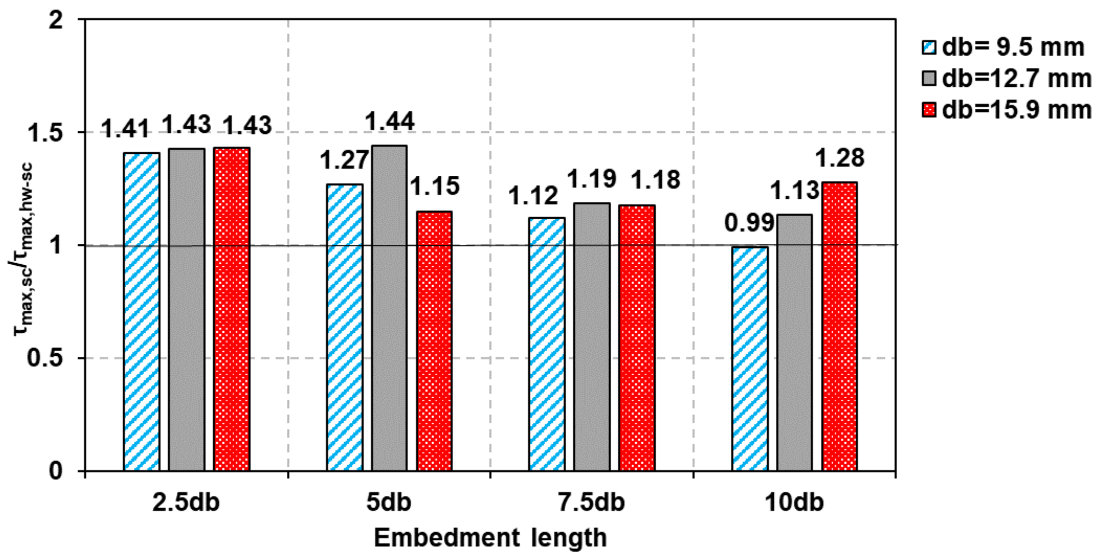

Figure 17. Comparison between bond strength of GFRP (SC) bars and bond strength of GFRP (HW-SC) bars for HSC cubes

4 Comparison of test results with current codes

For comparison purposes, the bond strengths provided by code equations were determined based on the geometrical and mechanical properties of the pull-out cubes. The ACI-440.1R [21] code proposed an equation for GFRP bars based on the work conducted by Wambeke and Shield [38] as below:

$$\frac{\tau_{max}}{0.083\sqrt{f_c'}} = 4 + 0.3\frac{\mathrm{c}}{\mathrm{d_b}} + 100\frac{\mathrm{d_b}}{\mathrm{l_e}} \quad (4)$$

where τ_{max} is the bond strength (MPa), f_c' is the cylinder compressive strength of concrete (MPa) and c is the lesser of the cover to the centre of the bar or one-half of the centre-to-centre spacing of the bars being developed (mm). The ratio of $\mathrm{c}/\mathrm{d_b}$ is limited to be less than 3.5. The CAN/CSA-S806 [22] and CAN/CSA-S6 [23] Canadian codes have also proposed the expressions for estimating the development length of FRP bars in conventional concrete in order to avoid bond failure. These equations were substituted in equation 1 to produce the expressions 5 and 6 for CAN/CSA-S806 and CAN/CSA-S6, respectively, which are used to calculate bond strength.

$$\tau_{max} = \frac{\mathrm{d_{cs}}\sqrt{\mathrm{f_c'}}}{1.15\mathrm{k_1k_2k_3k_4k_5}\pi d_b} \quad (5)$$

$$\tau_{max} = \frac{\left(\mathrm{d_{cs}} + \mathrm{k_{tr}}\frac{\mathrm{E_{frp}}}{\mathrm{E_s}}\right)\mathrm{f_{cr}}}{0.45\mathrm{k_1k_6}\pi d_b} \quad (6)$$

where:

$$k_{tr} = \frac{A_{tr}f_{yt}}{10.5sn} \qquad and \qquad \left(d_{cs} + k_{tr}\frac{E_{frp}}{E_s}\right) \leq 2.5d_b$$

where **k_1** is a bar location factor (1.3 for horizontal reinforcement placed so that more than 300 mm of fresh concrete is cast below the development length or splice, 1.0 for other cases), **k_2** is a concrete density factor (1.3 for structural low-density concrete, 1.2 for structural semi-low-density concrete, 1.0 for normal density concrete), **k_3** is a bar size factor (0.8 for $A_b \leq$ 300 mm^2, 1.0 for $A_b >$ 300 mm^2), $\mathbf{A_b}$ is the cross-sectional area of FRP bar (mm^2), **k_4** is a bar fibre factor (1.0 for GFRP), **k_5** is a bar surface factor (1.0 for surface-roughened or sand-coated surfaces and 1.05 for spiral pattern surface), **k_6** is a bar surface factor, being the ratio of the bond strength of the FRP bar to that of a steel deformed bar with the same cross-sectional area as the FRP bar, but not greater than 1.0. In the absence of experimental data, k_6 shall be taken as 0.8, $\mathbf{d_{cs}}$ is the smaller of the cover to the centre of the bar or two-thirds of the centre-to-centre spacing of the bars being developed (mm) (not greater than 2.5 $\mathrm{d_b}$), $\boldsymbol{k_{tr}}$ is a transverse reinforcement index, $\boldsymbol{A_{tr}}$ is the cross-sectional area of transverse reinforcement (mm^2), **s** is the maximum spacing centre to centre of the transverse bars within l_d (mm), $\boldsymbol{f_{yt}}$ is the yield stress in the transverse reinforcement (MPa), **n** is the number of bars being developed along the potential plane of bond splitting, $\boldsymbol{f_{cr}}$ is the cracking strength of concrete (MPa) ($0.4\sqrt{f_c'}$ for normal-density concrete, $0.34\sqrt{f_c'}$ for semi-low-density concrete, $0.3\sqrt{f_c'}$ for low-density concrete), $\mathbf{E_{frp}}$ and $\mathbf{E_s}$ are the modulus of elasticity of FRP and steel bars, respectively. The square root of concrete strength should be less than 5 and 8 MPa for CSA-S806 and CSA-S6, respectively.

The Japanese Design Code [24] suggested equation 7 to evaluate the bond strength of FRP bars to concrete:

$$\tau_{max} = \frac{f_{bod}}{\alpha_1} \tag{7}$$

where:

$$f_{bod} = 0.28\alpha_2 f_c'^{2/3}/1.3 \quad \leq 3.2\ N/mm^2$$

where $\boldsymbol{f_{bod}}$ is the design bond strength of concrete (MPa), $\boldsymbol{\alpha_2}$ is the modification factor for the bond strength of CFRM (= 1 when the bond strength of CFRM is equal to or greater than that of the deformed steel bars); otherwise α_2 shall be decreased according to the test results, $\boldsymbol{\alpha_1}$ is a confinement modification factor (= 1 when $k_c \leq 1$; 0.9 when $1 < k_c \leq 1.5$; 0.8 when $1.5 < k_c \leq 2$; 0.7 when $2 < k_c \leq 2.5$ and 0.6 when $k_c > 2.5$), k_c is specified as $\left(= \frac{c}{d_b} + \frac{15A_{tr}}{sd_b} + \frac{E_t}{E_s}\right)$, **c** is the smaller of the bottom clear cover of the main reinforcement or half of the clear space between the reinforcement being developed (mm), $\boldsymbol{A_{tr}}$ is the cross-sectional area of the transverse reinforcement (mm^2), **s** is the maximum spacing centre to centre of the transverse bars within l_{db} (mm), $\boldsymbol{E_t}$ is Young's modulus of elasticity for the transverse reinforcement (MPa) and $\boldsymbol{E_s}$ is Young's modulus for steel (MPa).

Tables 6 and 7 summarize the comparative results of the experimental bond strengths of various specimens with the predicted bond strengths calculated from the methods provided in ACI 440.1R-15, CSA-S806-12, CSA-S6-14 and JSCE [24]. In Figure 18 (a to c), the predictions provided by the ACI 440.1R, CSA-S806, CSA-S6 and JSCE equations were plotted using the geometrical and mechanical properties of the pull-out cube in the present study. It can be seen that the ACI 440.1R code overestimates the bond strength of both GFRP bars having an embedment length of 2.5d_b, while it is conservative for larger embedment lengths. The average ratio of experimental to predicted bond strengths obtained from the ACI 440.1R code is 1.06 with a COV of 34.3% and 1.45 with a COV of 25.6 for GFRP (type A) and GFRP (type B) reinforced cubes, respectively. CSA-S806, CSA-S6 and JSCE codes are too conservative, where the average ratios of experimental to predicted bond strengths for GFRP (type A) reinforced cubes are 4.41, 2.56 and 3.4 with a COV of 10.9%, respectively. They are 5.26, 3.21 and 4.26 with a COV of 17.4% for GFRP (type B) reinforced cubes. Tables 6 and 7 show that the bond strength obtained from Canadian and Japanese codes is not influenced by bar diameter and embedment length because of the limitations of d_{cs} and k_c in the Canadian and Japanese codes, respectively, as well as ignoring the effect of the embedment length on bond strength in both codes. This conclusion was also confirmed by Hossain et al. [13], by comparing test results with the Canadian code predictions. In contrast to the Canadian codes, the bond strength reduces with increasing embedment length as per the ACI 440.1R code. No change was noted in the ACI 440.1R predictions for identical specimens with the only one variable being bar diameter, and this is due to the limitation of the ratio of c/d_b and the value of the embedment length, that was taken as the ratio of the bar diameter, and this led to cancel the effect of bar diameter represented by d_b/l_e. However, from Tables 6 and 7, there is a slight change in bond strength with the increase of bar diameter for the cubes with the same embedment length, because of a small variation of concrete strength. The ACI 440.1R code does not acknowledge the influence of surface properties on bond strength. However, experimental results of GFRP (type A) and GFRP (type B) reinforced specimens plotted in Figure 18 (a) revealed that bond strength of GFRP (type B) bars is slightly higher than that of GFRP (type A) bars owing to the difference of surface configuration. It was noticed that the tested results for helical wrapped with slightly sand coated GFRP bars were closer to the ACI 440.1R predicted curve than the tested results for sand coated GFRP (SC) bars. This may be attributed to the fact that the ACI 440.1R equation was developed based on existing database containing limited surface types of only two (spiral wrapping and helical lugs). The Japanese design code also neglects the effect of surface configuration on bond strength. On the contrary, the Canadian codes acknowledge the effect of bar surface on bond strength by suggesting a bar surface factor of k_5 in the CSA-S806 equation and k_6 in the CSA-S6 equation. The ACI 440.1R equation was developed based on concrete strength in the range of 28 to 45 MPa [38]. Therefore, it cannot be assumed to be accurate for predicting the bond strength of GFRP bars in HSC. The Canadian code limitations regarding concrete strength ($\sqrt{f_c'}$ should not be more than 5 and 8 MPa for CSA-S806 and CSA-S6, respectively) and concrete cover (d_{cs} is not greater than $2.5d_b$) lead to a constant value of the predicted bond strength for all specimens as illustrated in Figure 18 (b). The modification factor, α_2, in the Japanese equation was taken as 1. According to the Japanese code limitation regarding the design bond strength of concrete, the predicted bond strength is constant when the concrete strength exceeds 57 MPa as shown in Figure 18 (c). Because of the absence of transverse reinforcement in the pull-out cubes, the effect of confinement considered by the transverse reinforcement index, k_{tr}, in the CSA S6 equation and the transverse reinforcement in the JSCE equation was neglected. The minimum value of the bond strength in experimental results is higher than the bond strengths obtained from Canadian and Japanese design codes, thus, the development length provided by these codes will be over satisfactory.

Table 6. Comparison of test results of GFRP (type A) reinforced cubes with different code's predictions

Specimen label	τ_{exp} **(MPa)**	**ACI 440.1R** τ_{pred} **(MPa)**	$\frac{\tau_{exp}}{\tau_{pred}}$	**CSA-S806** τ_{pred} **(MPa)**	$\frac{\tau_{exp}}{\tau_{pred}}$	**CSA-S6** τ_{pred} **(MPa)**	$\frac{\tau_{exp}}{\tau_{pred}}$	**JSCE 1997** τ_{pred} **(MPa)**	$\frac{\tau_{exp}}{\tau_{pred}}$
A-9.5-2.5d	20.55	34	0.60	4.11	5	7.07	2.91	5.33	3.85
A-9.5-5d	20.08	18.91	1.06	4.11	4.89	7.07	2.84	5.33	3.77
A-9.5-7.5d	19.76	13.88	1.42	4.11	4.81	7.07	2.79	5.33	3.71
A-9.5-10d	19.27	11.36	1.70	4.11	4.69	7.07	2.73	5.33	3.61
A-12.7-2.5d	19.79	34.07	0.58	4.11	4.82	7.07	2.80	5.33	3.71
A-12.7-5d	16.13	18.95	0.85	4.11	3.92	7.07	2.28	5.33	3.02
A-12.7-7.5d	16.71	13.90	1.20	4.11	4.07	7.07	2.36	5.33	3.13
A-12.7-10d	16.05	11.38	1.41	4.11	3.91	7.07	2.27	5.33	3.01
A-15.9-2.5d	19.42	34.76	0.56	4.11	4.73	7.07	2.75	5.33	3.64
A-15.9-5d	18.70	19.33	0.97	4.11	4.55	7.07	2.64	5.33	3.51
A-15.9-7.5d	16.32	14.23	1.15	4.11	3.97	7.07	2.31	5.33	3.06
A-15.9-10d	14.82	11.65	1.27	4.11	3.61	7.07	2.10	5.33	2.78
Average			1.06		4.41		2.56		3.40
COV %			34.3		10.9		10.9		10.9

Note: τ_{exp} is the experimental bond strength; τ_{pred} is the predicted bond strength and COV is a Coefficient of variation.

Table 7. Comparison of test results of GFRP (type B) reinforced cubes with different code's predictions

Specimen label	τ_{exp} (MPa)	ACI 440.1R τ_{pred} (MPa)	$\frac{\tau_{exp}}{\tau_{pred}}$	CSA-S806 τ_{pred} (MPa)	$\frac{\tau_{exp}}{\tau_{pred}}$	CSA-S6 τ_{pred} (MPa)	$\frac{\tau_{exp}}{\tau_{pred}}$	JSCE 1997 τ_{pred} (MPa)	$\frac{\tau_{exp}}{\tau_{pred}}$
B-9.5-2.5d	28.91	31.42	0.92	4.32	6.69	7.07	4.09	5.33	5.42
B-9.5-5d	25.51	16.89	1.51	4.32	5.91	7.07	3.61	5.33	4.78
B-9.5-7.5d	22.15	12.40	1.79	4.32	5.13	7.07	3.13	5.33	4.15
B-9.5-10d	19.05	10.15	1.88	4.32	4.41	7.07	2.69	5.33	3.57
B-12.7-2.5d	28.26	30.78	0.92	4.32	6.54	7.07	4.00	5.33	5.30
B-12.7-5d	23.21	17.12	1.36	4.32	5.37	7.07	3.28	5.33	4.35
B-12.7-7.5d	19.83	12.38	1.60	4.32	4.59	7.07	2.80	5.33	3.72
B-12.7-10d	18.18	10.14	1.79	4.32	4.21	7.07	2.57	5.33	3.41
B-15.9-2.5d	27.77	30.34	0.92	4.32	6.43	7.07	3.93	5.33	5.21
B-15.9-5d	21.52	16.87	1.28	4.32	4.98	7.07	3.04	5.33	4.04
B-15.9-7.5d	19.23	12.38	1.55	4.32	4.45	7.07	2.72	5.33	3.61
B-15.9-10d	18.93	10.14	1.87	4.32	4.38	7.07	2.68	5.33	3.55
Average			1.45		5.26		3.21		4.26
COV %			25.6		17.4		17.4		17.4

Note: τ_{exp} is the experimental bond strength; τ_{pred} is the predicted bond strength and COV is a Coefficient of variation.

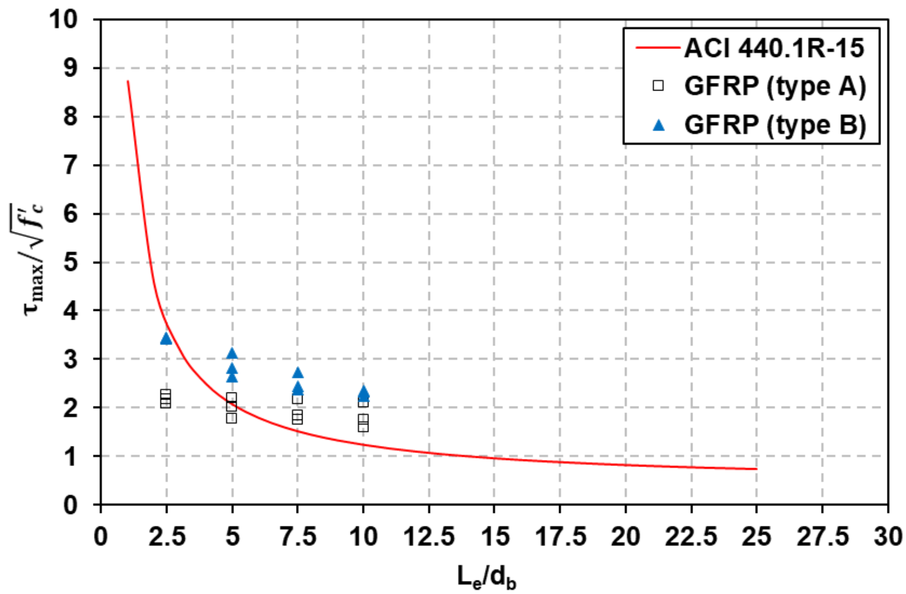

(a) Variation of normalized bond strength with embedment length

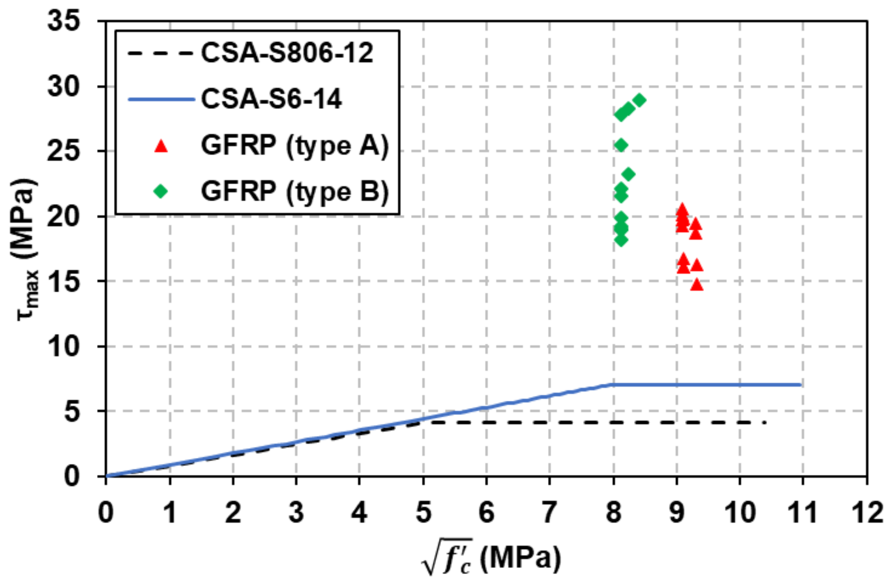

(b) Variation of bond strength vs. $\sqrt{f'_c}$

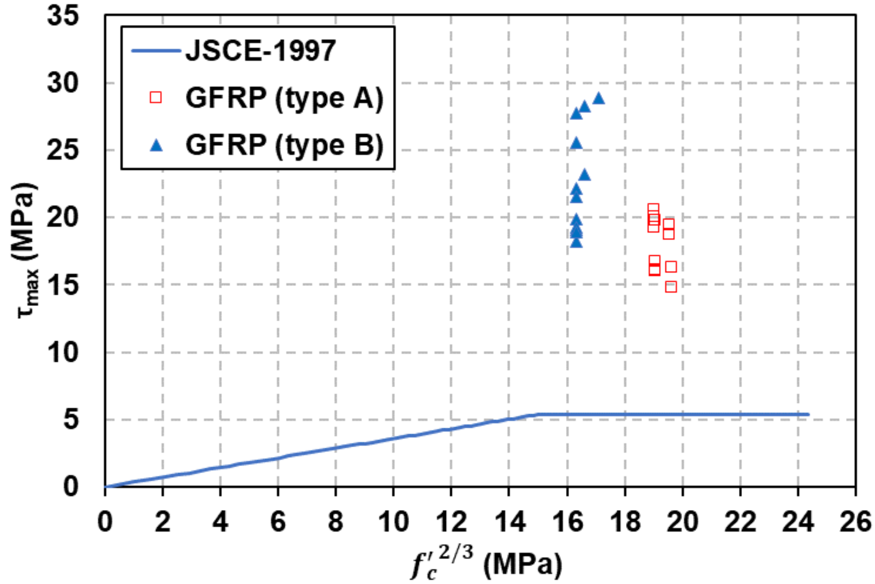

(c) Variation of bond strength vs. $f_c'^{2/3}$

Figure 18. Comparison between experimental and different design code predicted bond strengths for cubes

5 Conclusions

Test results of 84 HSC pull-out specimens reinforced with GFRP and steel bars have been presented and discussed in this paper. The parameters investigated were diameter, embedment length and surface configuration of the reinforcing bars. The following conclusions are drawn:

- The majority of specimens failed by a pull-out mode. The bond failure of GFRP (HW-SC) reinforced specimens occurred within the interfaces of the resin-rich layer and fibres, while it occurred within the interfaces between the sand coated layer and the bar core in GFRP (SC) reinforced specimens. The shearing off of concrete between the steel ribs was responsible for a pull-out failure in control specimens.
- GFRP (HW-SC) bars showed interfacial bond behaviour differing from that of GFRP (SC) bars. A helically wrapped with slightly sand coated surface produced a

more ductile post peak response with high residual stresses owing to high friction forces between remaining undulations and concrete, similar to previous observations in the literature for normal-strength concrete. A sand coated surface produced a brittle failure because of the complete stripping of sand grains from the bar core, unlike the literature (a smoother softening curve in the case of normal strength concrete).

- Overall, the bond strength of both GFRP types increased with reducing the embedment length and bar diameter.
- In general, the reduction rate of bond strength of both GFRP types with increasing the bar diameter and the embedment length was reduced in the case of high-strength concrete.
- The sand coated surface offered a bond strength higher than that offered by the helically wrapped with slightly sand coated surface for a given concrete strength, but the corresponding slip for GFRP (SC) bars was less than that for GFRP (HW-SC) bars.
- In general, all design codes provided conservative predictions, but ACI predictions were unconservative for pull-out cubes having an embedment length of $2.5d_b$. ACI predictions showed a good agreement with experimental bond strengths compared to other codes.
- Both Canadian and Japanese codes are overly safe. Therefore, modifications to these codes are necessary for a more accurate prediction of bond strength of GFRP bars embedded in HSC.

Acknowledgement

The first Author would like to acknowledge to the financial support of Higher Education of Libya (293/2013). The authors are also gratefully to PULTRALL & V.ROD for providing the GFRP (SC) bars, and Hughes brother's manufacturer and Fortius, Belgium Vendor for providing the ASLAN 100 GFRP (HW-SC) bars.

References

1. Achillides, Z. and K. Pilakoutas, Bond behaviour of fibre reinforced polymer bars under direct pullout conditions. Journal of Composites for Construction, 2004. 8(2): p. 173-181.
2. Okelo, R. and R.L. Yuan, Bond strength of fibre reinforced polymer rebars in normal strength concrete. Journal of composites for construction, 2005. 9(3): p. 203-213.
3. Tastani, S. and S. Pantazopoulou, Bond of GFRP bars in concrete: experimental study and analytical interpretation. Journal of Composites for Construction, 2006. 10(5): p. 381-391.
4. Hao, Q.-d., Y.-l. Wang, Z.-c. Zhang, and J.-p. Ou, Bond strength improvement of GFRP rebars with different rib geometries. Journal of Zhejiang University SCIENCE A, 2007. 8(9): p. 1356-1365.
5. Baena, M., L. Torres, A. Turon, and C. Barris, Experimental study of bond behaviour between concrete and FRP bars using a pull-out test. Composites Part B: Engineering, 2009. 40(8): p. 784-797.
6. Hao, Q., Y. Wang, Z. He, and J. Ou, Bond strength of glass fibre reinforced polymer ribbed rebars in normal strength concrete. Construction and Building materials, 2009. 23(2): p. 865-871.
7. El Refai, A., M.-A. Ammar, and R. Masmoudi, Bond performance of basalt fibre-reinforced polymer bars to concrete. Journal of Composites for Construction, 2014. 19(3): p. 04014050.
8. Xue, W., Q. Zheng, Y. Yang, and Z. Fang, Bond behaviour of sand-coated deformed glass fibre reinforced polymer rebars. Journal of Reinforced Plastics and Composites, 2014. 33(10): p. 895-910.
9. Benmokrane, B., O. Chaallal, and R. Masmoudi, Glass fibre reinforced plastic (GFRP) rebars for concrete structures. Construction and Building Materials, 1995. 9(6): p. 353-364.
10. Lee, J.-Y., T.-Y. Kim, T.-J. Kim, C.-K. Yi, J.-S. Park, Y.-C. You, and Y.-H. Park, Interfacial bond strength of glass fibre reinforced polymer bars in high-strength concrete. Composites Part B: Engineering, 2008. 39(2): p. 258-270.
11. Davalos, J.F., Y. Chen, and I. Ray, Effect of FRP bar degradation on interface bond with high strength concrete. Cement and Concrete Composites, 2008. 30(8): p. 722-730.
12. Lee, J.Y., C.K. Yi, Y.G. Cheong, and B.I. Kim, Bond stress–slip behaviour of two common GFRP rebar types with pullout failure. Magazine of Concrete Research, 2012. 64(7): p. 575-591.
13. Hossain, K.M.A., D. Ametrano, and M. Lachemi, Bond Strength of Standard and High-Modulus GFRP Bars in High-Strength Concrete. Journal of Materials in Civil Engineering, 2014. 26(3): p. 449-456.

14. Tekle, B.H., A. Khennane, and O. Kayali, Bond Properties of Sand-Coated GFRP Bars with Fly Ash–Based Geopolymer Concrete. Journal of Composites for Construction, 2016. 20(5): p. 1-13.
15. Lee, J.-Y., A.-R. Lim, J. Kim, and J. Kim, Bond behaviour of GFRP bars in high-strength concrete: bar diameter effect. Magazine of Concrete Research, 2017. 69(11): p. 541-554.
16. Tighiouart, B., B. Benmokrane, and D. Gao, Investigation of bond in concrete member with fibre reinforced polymer (FRP) bars. Construction and Building Materials, 1998. 12(8): p. 453-462.
17. Chaallal, O. and B. Benmokrane, Pullout and bond of glass-fibre rods embedded in concrete and cement grout. Materials and structures, 1993. 26(3): p. 167-175.
18. Veljkovic, A., V. Carvelli, M.M. Haffke, and M. Pahn, Concrete cover effect on the bond of GFRP bar and concrete under static loading. Composites Part B: Engineering, 2017. 124: p. 40-53.
19. Harajli, M. and M. Abouniaj, Bond performance of GFRP bars in tension: Experimental evaluation and assessment of ACI 440 guidelines. Journal of Composites for Construction, 2010. 14(6): p. 659-668.
20. Esfahani, M.R., M. Rakhshanimehr, and S.R. Mousavi, Bond Strength of Lap-Spliced GFRP Bars in Concrete Beams. Journal of Composites for Construction, 2013. 17(3): p. 314-323.
21. ACI-440.1R, Guide for the design and construction of concrete reinforced with FRP bars. 2015, ACI Committee 440: Farmington Hills, M1.
22. CAN/CSA-S806, Design and construction of building structures with fibre-reinforced polymers. 2012, Canadian Standards Association: Mississauga, Ontario, Canada.
23. CAN/CSA-S6, Canadian Highway Bridge Design Code. 2014, Canadian Standard Association.
24. JSCE, Recommendation for Design and Construction of Concrete Structures using Continuous Fibre Reinforcing Materials. 1997, Research Committee Fibre-Reinforcing Materials: Tokyo, Japan.
25. ACI-440.3R, Guide Test Methods for Fibre-Reinforced Polymers (FRPs) for Reinforcing or Strengthening Concrete Structures. 2012, ACI Committee 440: Farmington Hills, M1.
26. ASTM-D7205/D7205M-06, Standard test method for tensile properties of fibre reinforced polymer matrix composite bars. 2006, ASTM International: West Conshohocken, United States. p. 13.
27. ASTM-A706/A706M-09b, Standard Specification for Low-Alloy Steel Deformed and Plain Bars for Concrete Reinforcement. 2009, ASTM International: West Conshohocken, United States. p. 6.

28. Vint, L. and S. Sheikh, Investigation of Bond Properties of Alternate Anchorage Schemes for Glass Fibre-Reinforced Polymer Bars. ACI Structural Journal, 2015. 112(1): p. 59.
29. Antonietta Aiello, M., M. Leone, and M. Pecce, Bond performances of FRP rebars-reinforced concrete. Journal of materials in civil engineering, 2007. 19(3): p. 205-213.
30. Arias, J.P.M., A. Vazquez, and M.M. Escobar, Use of sand coating to improve bonding between GFRP bars and concrete. Journal of composite materials, 2012. 46(18): p. 2271-2278.
31. Pepe, M., H. Mazaheripour, J. Barros, J. Sena-Cruz, and E. Martinelli, Numerical calibration of bond law for GFRP bars embedded in steel fibre-reinforced self-compacting concrete. Composites Part B: Engineering, 2013. 50: p. 403-412.
32. Nanni, A., M. Al-Zaharani, S. Al-Dulaijan, C. Bakis, and I. Boothby. bond of FRP reinforcement to concrete-experimental results. in Non-Metallic (FRP) Reinforcement for Concrete Structures: Proceedings of the Second International RILEM Symposium. 1995. CRC Press.
33. Benmokrane, B., B. Tighiouart, and O. Chaallal, Bond strength and load distribution of composite GFRP reinforcing bars in concrete. ACI Materials Journal, 1996. 93(3): p. 246-252.
34. Cosenza, E., G. Manfredi, and R. Realfonzo, Behaviour and modeling of bond of FRP rebars to concrete. Journal of composites for construction, 1997. 1(2): p. 40-51.
35. Achillides, Z., Bond behaviour of FRP bars in concrete, in Dept. of Civil and Structural Engineering. 1998, University of Sheffield: Sheffield, U.K.
36. Tepfers, R., Bond clause proposals for FRP bars/rods in concrete based on CEB/FIP Model Code 90. Part 1: Design bond stress for FRP reinforcing bars. Structural concrete, 2006. 7(2): p. 47-55.
37. Xue, W., X. Wang, and S. Zhang, Bond properties of high-strength carbon fibre-reinforced polymer strands. ACI Materials Journal, 2008. 105(1): p. 11-19.
38. Wambeke, B.W. and C.K. Shield, Development length of glass fibre-reinforced polymer bars in concrete. ACI Structural Journal, 2006. 103(1): p. 11-17.

Abbreviations

GFRP Glass Fibre Reinforced Polymers
HW-SC Helical Wrapping with slightly Sand Coating
SC Sand Coating
CFRM Continuous Fibre Reinforcing Materials
NSC Normal Strength Concrete
HSC High Strength Concrete

ACI American Concrete Institute
ASTM American Society for Testing and Materials
JSCE Japanese Society of Civil Engineers
CSA Canadian Standards Association
COV Coefficient of Variation
LVDT Linear Variable Displacement Transducer
PO Pull-out
SP Splitting
Y Yielding

Notations

d_b Bar diameter
L_e Embedment length
L_{db} Development length
L_a Length from the LVDTs support point to the top surface of the bonded bar
A_b Cross sectional area of bar
A_t Cross-sectional area of transverse reinforcement
f_c' Cylinder compressive strength of concrete
f_{cu} Cube compressive strength of concrete
f_t Tensile strength of concrete
f_{cr} Cracking strength of concrete
E_{frp} Elastic modulus of FRP rebar
E_s Elastic modulus of steel rebar
α_1 Confinement modification factor
α_2 Modification factor for bond strength
f_{bod} Design bond strength of concrete
E_t Young's modulus of elasticity for the transverse reinforcement
f_{yt} Yield stress in transverse reinforcement
k_1 Top bar modification factor
k_2 Concrete density factor
k_3 Bar size factor
k_4 Bar fibre factor
k_5 Surface profile factor
k_6 Bar surface factor
k_{tr} Transverse reinforcement index
C The lesser of the concrete cover to the centre of the bar or one-half of the centre-to-centre spacing of the bars being developed
d_{cs} The smaller of the distance from the closest concrete surface to the centre of the bar or two-thirds of the centre to centre spacing of the bars

s	Maximum spacing centre to centre of transverse bars within l_{db}
n	Number of bars being developed along the potential plane of bond splitting
τ_{max}	Peak bond stress
τ	Bond stress
τ_{avg}	Average bond strength
τ_{pred}	Predicted bond strength
τ_{exp}	Experimental bond strength
F	Applied tensile load
F_{max}	Failure load
s_{le}	Loaded end slip at the peak bond stress
s_{ul}	Unloaded end slip at the peak bond stress
s_e	Elongation of the bar
s_{total}	LVDT measurement at the loaded end
$s_{le,m}$	Average loaded end slip at the peak bond stress
$s_{ul,m}$	Average unloaded end slip at the peak bond stress